THE GEOLOGICAL SOCIETY OF AMERICA®

Late Miocene expansion of grasslands in northwest Argentina linked to shifting hydroclimate: A complex interaction among tectonics, climate, and ecology

Iffat Azmi[1,†], Ethan Hyland[1], Jennifer Cotton[2], Adit Ghosh[2,3], Maria Sol Raigemborn[4], David Tineo[4], Scott Hauswirth[2], and Nadja Insel[5]

[1]*Department of Marine, Earth, and Atmospheric Sciences, North Carolina State University, Raleigh, North Carolina 27695, USA*
[2]*Department of Geological Sciences, California State University–Northridge, Northridge, California 91330, USA*
[3]*Department of Earth Sciences, University of Southern California, Los Angeles, California 90089, USA*
[4]*Centro de Investigaciones Geologicas, Consejo Nacional de Investigaciones Científicas y Técnicas (CONICET)–Universidad Nacional de La Plata, B1900 La Plata, Provincia de Buenos Aires, Argentina*
[5]*Department of Earth Science, Northeastern Illinois University, Chicago, Illinois 60625, USA*

ABSTRACT

Factors driving the late Miocene expansion of C_4 grasses remain widely debated. Here, we explored the role of climate and fire in controlling the abundance of C_4 vegetation in the Angastaco Basin (Palo Pintado area) and La Viña Basin, NW Argentina, during the late Miocene (ca. 14–5.33 Ma). From paleosol horizons, we reconstructed paleoclimate and paleovegetation conditions using phytolith assemblages, geochemical and isotopic proxies, and polycyclic aromatic hydrocarbons (PAHs) to determine fire input. Our paleoclimate reconstructions suggest a stable mean annual temperature (MAT) of ~10 °C and a gradual decline in mean annual precipitation (MAP) from 1100 mm yr^{-1} to 850 mm yr^{-1}. Paleovegetation reconstructions from carbon isotopic composition and phytolith assemblages show a maximum of ~15% C_4 vegetation by 6 Ma. No significant increases in fire occurrence or establishment of fire feedbacks were identified from the PAH data. Though low in abundance (~3% on average), our data identified the presence of C_4 grass by the late Miocene. The lack of significant C_4 expansion in this region was likely controlled by the changing hydroclimatic conditions associated with the Andes mountain range—increasing aridity and elevation constraints along with the lack of a fire feedback might have limited the distribution of C_4 vegetation.

1. INTRODUCTION

The Miocene Epoch (23–5 Ma) is an interval in Earth's history that was slightly warmer than today and has been referred to as "the future of the past" (Steinthorsdottir et al., 2021) due to its importance for future projections of anthropogenic climate change. Global climate was ~3–7 °C warmer than present (e.g., Westerhold et al., 2020; Steinthorsdottir et al., 2021), while atmospheric carbon dioxide concentrations (pCO_2) ranged from ~380 ppm to 710 ppm, comparable to the modern values (Balcerak, 2011; Beerling and Royer, 2011; Knorr et al., 2011) and predicted changes by 2100 (IPCC, 2014). Modern global tectonic and topographic configurations also started to take shape during this period, and floral and faunal communities experienced a series of shifts toward the development of modern ecosystems; one of these key transitions was the evolution and expansion of C_4 grasslands (e.g., Edwards et al., 2010; Strömberg, 2011; Herbert et al., 2016). In modern ecosystems, C_4 grasses are mostly found at low latitudes and low elevations (Sage, 2001) and account for 18%–23% of gross primary production (Still et al., 2003; Luo et al., 2024), making them an essential part of the global carbon cycle. Ongoing anthropogenic climate change, characterized by rising pCO_2 levels, increased temperatures, and altered precipitation patterns, can significantly impact the distribution of C_4 grasslands and their carbon storage dynamics (Luo et al., 2024). Therefore, understanding the expansion of C_4 grasses in the late Miocene is crucial for predicting their response to future anthropogenic changes.

The three primary photosynthetic pathways used in plants are C_3, C_4, and Crassulacean acid metabolism (CAM). C_4 photosynthesis is a specialized adaptation that evolved to enhance photosynthetic efficiency under high temperatures and low atmospheric CO_2 concentrations (Ehleringer and Cerling, 2002; Raghavendra and Sage, 2010) by suppressing photorespiration—a limitation of the ancestral C_3 photosynthetic pathway (Leegood, 2000). C_4 photosynthesis involves two stages in which a four-carbon molecule (oxaloacetate [OAA]) is produced by binding CO_2 with phosphoenolpyruvate (PEP) in the mesophyll cell, and then OAA reduces into malate; subsequent decarboxylation creates a CO_2-rich environment for ribulose-1,5-bisphosphate carboxylase/oxygenase (RubisCO) in the bundle sheath cells (Ehleringer and Cerling, 2002; Gowik and Westhoff, 2011). This unique pathway is suggested to have evolved as early as the Oligocene (e.g., Ehleringer et al., 1991; Sage, 2004; Pagani et al., 2005; Christin et al., 2012; Sage et al., 2012), and by the late Miocene, C_4 grasses had expanded into tropical, subtropical, and temperate grasslands worldwide at the expense of both forests and C_3 grasslands (Cerling et al., 1993; Edwards and Still, 2008; Edwards et al., 2010; Herbert et al., 2016).

Many factors have been proposed to explain the evolution and rapid expansion of C_4 grasslands during the late Miocene, yet the drivers and timing of the phenomenon are still debated.

Iffat Azmi https://orcid.org/0000-0002-1678-6269
[†]iazmi@ncsu.edu

GSA Bulletin;
published online 7 March 2025

https://doi.org/10.1130/B37868.1.

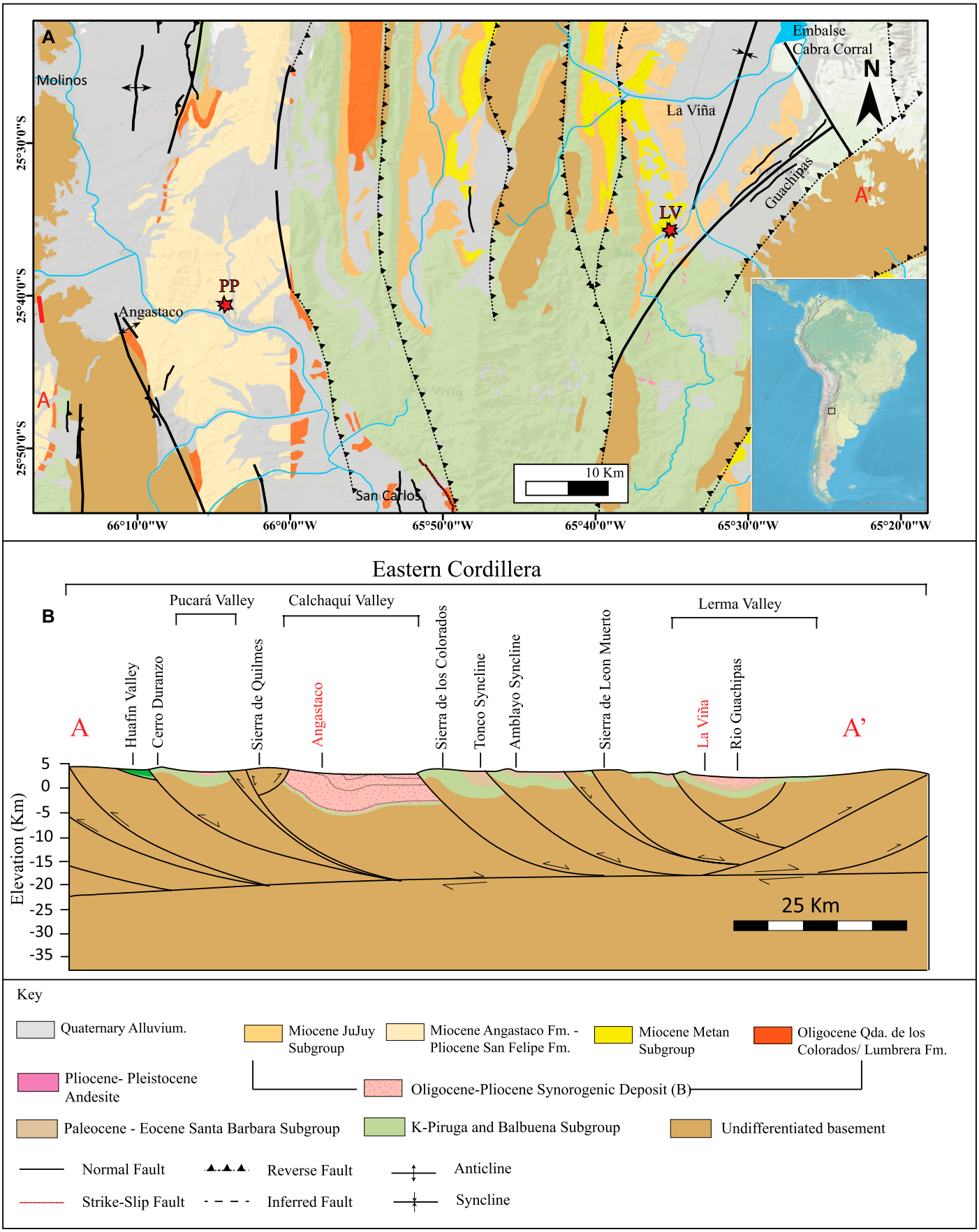

Figure 1. (A) Geological map of the greater Angastaco Basin in NW Argentina. Stars indicate sampling localities (PP—Palo Pintado Formation, Angastaco Basin; LV—La Viña Basin); black polygon in inset indicates study area. (B) Cross section along A–A′ (shown in A) illustrating general geology and major structures of Eastern Cordillera in NW Argentina (modified after Carrapa et al., 2011). Qda—Quebrada.

The debate centers on whether the expansion of C_4 plants was primarily driven by broad, global changes or by distinct, regional factors (e.g., Tauxe and Feakins, 2020). Proponents of globally driven changes suggest a broad global change in atmospheric and/or climatic conditions during the late Cenozoic (Lu et al., 2020). Cerling et al. (1997) proposed a CO_2 starvation hypothesis, suggesting declining pCO_2 during the late Miocene as a trigger for the expansion; however, this was subsequently abandoned due to the lack of proxy evidence for pCO_2 changes on these time scales (Pagani et al., 1999; Pearson and Palmer, 2000; Osborne, 2008), as well as evidence for both diachronous (e.g., Tauxe and Feakins, 2020) and regionally variable climatic responses to declining pCO_2 (e.g., Higgins and Scheiter, 2012). Instead, several other factors such as fire activities (Keeley and Rundel, 2005), wind strength (Tipple and Pagani, 2007), aridity (Saarinen et al., 2020), and other ecological disturbances (e.g., herbivory; Retallack, 2007; Osborne, 2008) were proposed, and the variable importance or interaction of these factors may help to explain the timeline and pace of C_4 expansions (e.g., Zhou et al., 2018).

Studies on modern C_4 grasses show that C_4 photosynthesis is favored in warm, dry, open habitats with high light conditions (Edwards and Smith, 2010), while phylogenetic analysis indicates that C_4 photosynthesis likely arose in monsoon-affected regions of warm-temperate to tropical latitudes (Sage et al., 2012). C_4-dominated ecosystems are favored by seasonal climates due to their temperature and precipitation gradients, water availability, and fire dynamics (Keeley and Rundel, 2005; Osborne and Beerling, 2005). These details, along with the spatiotemporal differences in the spread of C_4 grasslands as documented in different regions (Freeman and Colarusso, 2001; Hoetzel et al., 2013; Smiley et al., 2018; Hyland et al., 2019; Feakins et al., 2020), suggest the need to consider the local and regional climate in context. For instance, Quade et al. (1995) reported the late Miocene C_4 vegetation shift to be coincident with monsoon intensification due to the uplift of the Tibetan Plateau, which has been reinforced by additional work (e.g., Karp et al., 2018). Andrae et al. (2018) suggested that highly seasonal precipitation promoted by a summer monsoon during the late Pliocene favored C_4 expansion in Australia. In Africa, regional climate change has been attributed as the main driving force causing the C_4 expansion in the late Miocene–Pliocene (e.g., Dupont et al., 2013; Miao et al., 2022; Peppe et al., 2023).

Variations in the timing of expansion and local abundance of C_4 grasses in South America during the late Miocene highlight the challenges in exploring and understanding these driving mechanisms. Broadly, the timing of reported C_4 grass expansion from isotopic and fossil records from South America (Latorre et al., 1997) coincides with the evolution of the South American summer monsoon system (SASM). Rohrmann et al. (2016) suggested that the modern vegetation abundance reflects the climatic conditions of this region modulated by the SASM, warranting further exploration to understand the potential link between the evolution of the SASM and its impact on C_4 abundance. This study sought to evaluate the role of hydrological conditions and climatic shifts in shaping the C_4 vegetation conditions in northwest Argentina during the late Miocene. Based on links between seasonal precipitation and C_4 abundances elsewhere (e.g., Cotton et al., 2016; Andermann et al., 2022), we hypothesize that late Miocene C_4 grassland expansion, or the lack thereof, in this region was primarily controlled by shifting hydroclimate related to ongoing Andean orogenic processes. In addition to the climatic and tectonically driven topographic variations, we investigated the role of fire occurrence, which has been suggested as a possible secondary factor for promoting C_4 vegetation (Sage, 2001; Bond et al., 2003). In seasonal climates, a positive feedback loop between C_4 vegetation and fire activities is established by promoting C_4 grass growth and canopy clearing (Hatch, 1987; Ehleringer and Monson, 1993; Osborne and Beerling, 2005), which has been observed in modern grassland ecosystems (D'Antonio and Vitousek, 1992; Rossiter et al., 2003). Evidence of fire feedbacks facilitating and maintaining C_4 grasslands during the Miocene has been identified in South Asia (Karp et al., 2018, 2021a) and southern Africa (Hoetzel et al., 2013).

We reconstructed paleoclimate conditions, paleovegetation, and paleofire occurrence in northwest Argentina during the late Miocene using a multiproxy approach, including bulk geochemical and isotopic composition analyses of paleosol materials (B horizons, soil organic matter, pedogenic carbonates), along with extracted phytolith assemblages and polycyclic aromatic hydrocarbon (PAH) abundances. We used PAH biomarkers to reconstruct paleofire input and identify changes in fire regimes by comparing PAH measurements with paleoclimate and paleovegetation reconstructions to identify the link between climate and vegetation changes and the role of fire in these ecosystems.

2. GEOLOGICAL SETTING

2.1. Tectonic and Environmental Context

Cenozoic shortening of the South American plate overriding the Nazca plate with a moderate (30°) eastward dip (Horton, 2018) led to the formation of the Andean range along the west coast of South America (Sobolev et al., 2006; Ramos, 2009; DeCelles et al., 2011). During the Cenozoic, the orogenic front migrated eastward, leading to the evolution of a retroarc foreland basin located east of the central Andean topographic front, which hosts a thick accumulation of Cenozoic clastic sediments and paleosols (Chase et al., 2009; DeCelles et al., 2011). Once contiguous with the Paleogene retroarc foreland basin, extending from the Altiplano Puna Plateau to the Eastern Cordillera, the Angastaco Basin underwent deformation and subsequent separation from the Altiplano Puna Plateau at ca. 20 Ma (Coutand et al., 2006; Pingel et al., 2016). As deformation and exhumation progressed eastward, the uplift of the Sierra de Colorados ranges in the late Miocene separated the La Viña Basin from the Angastaco Basin (Fig. 1A). To the west, the Angastaco Basin is separated from the Altiplano Puna Plateau by N-S–striking, reverse fault–bounded ranges such as the Sierra Quilmes and Cerro Duranzo, and to the east by the ranges of the Sierra de los Colorados and Sierra León Muerto (Fig. 1B; Pingel et al., 2016). The eastern ranges form an effective orographic barrier that causes intense rainfall along the eastern flank and a semiarid to arid hinterland (Hain et al., 2011).

The Angastaco Basin hosts a very thick (>6 km) accumulation of Eocene through Pliocene terrestrial clastic sediments, comprising the Payogastilla Group (Díaz and Malizzia, 1983; Bywater-Reyes et al., 2010). This group is further subdivided into four formations: (1) the Quebrada de los Colorados, (2) the Angastaco, (3) the Palo Pintado, and (4) the San Felipe Formations (Coutand et al., 2006). The Quebrada de los Colorados Formation suggests a maximum depositional age of 37.6 ± 1.2 Ma, while the

overlying Angastaco Formation was deposited between ca. 21 Ma and 9 Ma (Carrapa et al., 2012). The next overlying Palo Pintado Formation is interpreted to be middle to late Miocene in age (Starck and Anzótegui, 2001; Bywater-Reyes et al., 2010) based on interbedded ash beds. The San Felipe Formation is gradational with the Palo Pintado Formation, and magnetostratigraphic data suggest it was deposited during ca. 5–2 Ma (Reynolds et al., 2000).

This study focused on the late Miocene Palo Pintado Formation in the Angastaco Basin and its equivalents (Jesús María, Guanaco, and Piquete Formations) within the La Viña Basin (Fig. 1). The Palo Pintado Formation lies conformably on the Angastaco Formation and can be divided into two sections: (1) the bottom 1500 m interval is composed of fine- to coarse-grained sandstone interlayered with siltstone and mudstone, and it is interpreted to have been deposited in a meandering fluvial system (Díaz and Malizzia, 1983); (2) the upper 450 m interval is composed of coarsening-upward sandstone interfingered with massive conglomerate and tuff beds, and it is interpreted to have been deposited in a braided fluvial system (Díaz and Malizzia, 1983). Petrographic data suggest that the Eastern Cordillera was the major source of these sediments at least between 14.5 Ma and 5 Ma (Coutand et al., 2006). Based on the sedimentological, paleontological, and isotopic values of pedogenic carbonate nodules from the Palo Pintado Formation, Bywater-Reyes et al. (2010) suggested that this deposition occurred during relatively humid intervals within a broadly semiarid climate. The overlying San Felipe Formation consists of cobble conglomerate and fining-upward sandstone and is correlated with the Piquete Formation in La Viña Basin. It is interpreted to be a braided stream and distal alluvial-fan deposit that reflects increased aridity compared to the underlying Palo Pintado Formation. Thus, based on these sedimentological interpretations, the Palo Pintado Formation marks an environmental change from dry conditions, reflected in the deposition of the Angastaco Formation (15–9 Ma), to humid conditions, with the transition suggested to have coincided with the onset of the SASM (Starck and Anzótegui, 2001; Coutand et al., 2006; Bywater-Reyes et al., 2010).

The Palo Pintado Formation has been correlated with the Jesús María and Guanaco Formations of the La Viña Basin, where Carrapa et al. (2012) studied a >1000-m-thick section. The Jesús María Formation is composed primarily of laminated and rippled mudstones, while the overlying Guanaco Formation is composed of red, tan, and brown silty mudstone and trough cross-bedded sandstones. The Piquete Formation, which is correlated to the San Felipe Formation (Carrapa et al., 2012), is composed of tan siltstone, sandstone, and conglomerates. Overall, these deposits are suggested to have had a fluviolacustrine origin (Carrapa et al., 2012), and the depositional age of these formations is somewhat constrained via radiometric and biostratigraphic data. Using zircon U-Pb geochronology of one ash layer from the Jesús María Formation, Carrapa et al. (2012) dated it to be 14.4 ± 0.6 Ma (A3 in Fig. 2). An additional K/Ar radiometric age of an ash bed from the Guanaco Formation (A4 in Fig. 2) suggested it to be 8.73 ± 0.25 Ma (Del Papa et al., 1993), while zircon U-Pb geochronology placed it at 9.31 ± 0.31 Ma (Hain et al., 2011). Based on

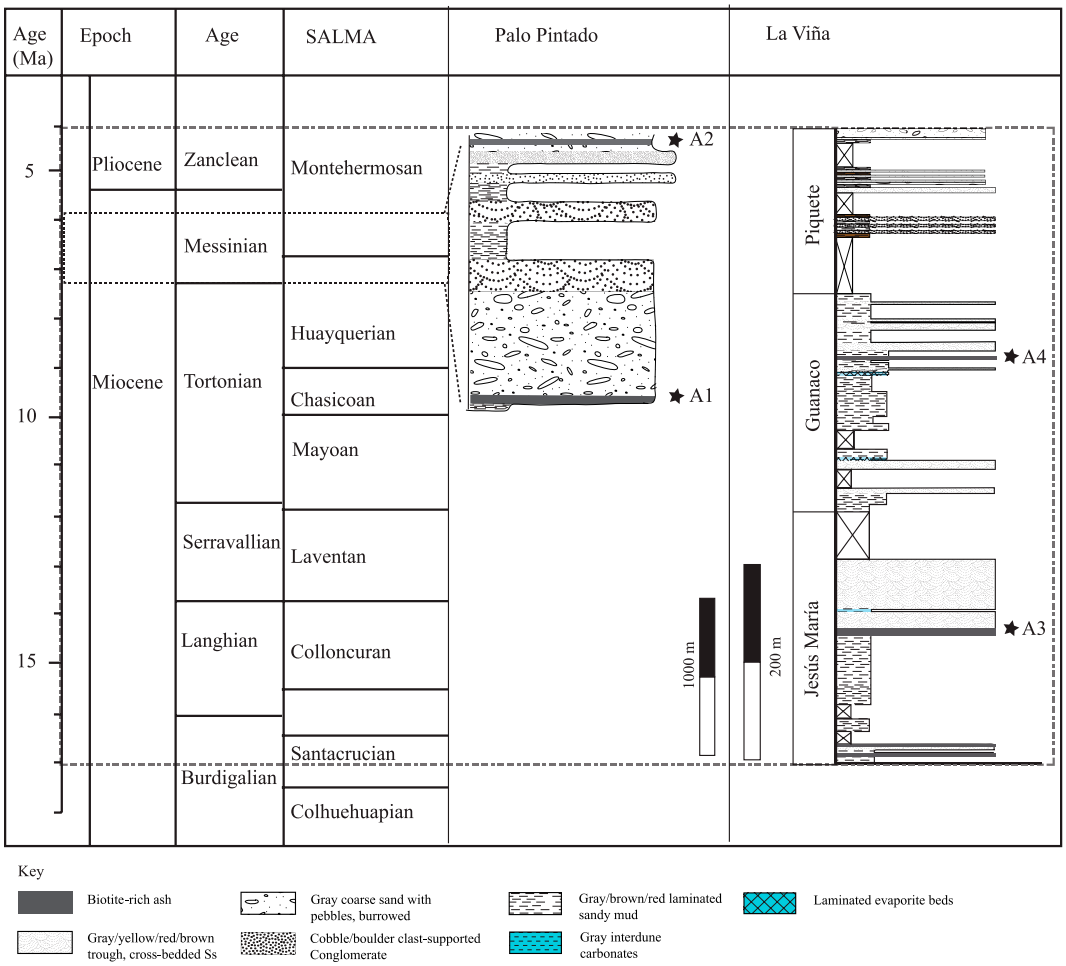

Figure 2. General stratigraphy of Palo Pintado Formation (Angastaco Basin) and La Viña Basin (scale bar indicates thickness in meters). SALMA—South American Land Mammal Age; Ss—sandstone.

previous studies from a different locality farther north, Ulberich et al. (2021) suggested that the temporal range for the Guanaco Formation can be constrained between ca. 10.9 Ma and ca. 5 Ma, while the age of the overlying Piquete Formation is estimated to be between ca. 5 Ma and 1.3 ± 0.2 Ma.

2.2. Age Model

Based on the previously obtained radiometric ages from these sections, we inferred a composite age model for both subbasins (e.g., Carrapa et al., 2011, 2012). Previous age models allow correlation between the Angastaco and La Viña Basins (Fig. 2), which were connected before the exhumation of the Sierra de los Colorados (Starck and Vergani, 1996; Bywater-Reyes et al., 2010; Carrapa et al., 2012). More specifically, the Palo Pintado Formation represents ca. 7.24–5.96 Ma (Bywater-Reyes et al., 2010) and corresponds to the Huayquerian–Montehermosan interval of the South American Land Mammal Age (SALMA) framework, as indicated by U-Pb zircon ages from the interbedded ash layers, which precisely bracket the formation and provide clear markers at 8 m and 1730 m in the section (Fig. 2). Compared to the Palo Pintado Formation, formations within La Viña Basin have a less constrained age model derived from two ash beds. Ash bed A3, found at 129 m in the Jesús María Formation, is correlated to the U-Pb zircon age of 14.4 ± 0.7 Ma (Carrapa et al., 2012), corresponding to the Santacrucian–Laventan interval of SALMA, and ash bed A4, at 411 m in the Guanaco Formation, correlates to the biotite K/Ar age of 8.73 ± 0.25 Ma (Del Papa et al., 1993; Fig. 2) in the Mayoan–Huayquerian interval.

Previous workers have assumed a uniform sedimentation rate for the La Viña Basin (consistent with biostratigraphic data and conformable formation boundaries; e.g., Bywater-Reyes et al., 2010; Carrapa et al., 2011), suggesting this section represents an interval between ca. 17 Ma and 4.1 Ma. The substantially higher sedimentation rate in the Angastaco Basin (~1300 m/m.y.) relative to La Viña Basin (~50 m/m.y.) is reasonable given their relative landscape/tectonic positions, with the Angastaco Basin receiving sediment directly from the Eastern Cordillera throughout the Miocene via fluvial and alluvial deposition in the proximal foreland basin, while La Viña Basin instead was shielded from sediment sources by the Sierra de los Colorados (e.g., Bywater-Reyes et al., 2010) and filled via slower fluvial and lacustrine deposition (see below) in the distal foreland basin. Considering the estimated ages and relative deposition rates of these formations, using the Palo Pintado Formation along with formations from the La Viña Basin allows us to create a composite record of basin settings and persisting paleoenvironmental conditions during ca. 17–5 Ma, with a higher-resolution record for the youngest end of this range (ca. 7–5 Ma).

3. METHODS

3.1. Sample Collection

Detailed field stratigraphy and facies descriptions were recorded for each locality, with particular attention paid to pedogenically modified zones. Paleosols were identified based on the presence of a wide variety of features, including horizonation, color changes/gleying, and complex burrows and root traces/rhizoliths, as well as pedogenic carbonate nodules and preserved ped structures. Paleosols were classified by pedotype based on the taxonomic classification schemes of the U.S. Department of Agriculture (Soil Survey Staff, 2014) and paleosol-specific conventions (Mack et al., 1993; Retallack, 2008). Paleosols were described, photographed, and measured in the field, and samples were collected for geochemical, isotopic, and phytolith analyses. To obtain fresh samples, weathered or pedogenically modified surface materials were removed carefully to depths >30 cm, and samples were collected from all available paleosol horizons, with specific attention paid to A and B horizons because they preserve the most phytoliths (A horizon; Strömberg, 2004), soil organic matter (A horizon; Cotton et al., 2014), and relevant geochemical signals (B horizon; Hyland and Sheldon, 2016).

3.2. Paleoclimate Reconstructions

Paleoclimate reconstructions were based on climofunctions derived from bulk geochemical analysis of 17 paleosol samples from the Angastaco Basin and 11 paleosol samples from the La Viña Basin. B horizon samples were selected for these analyses, and samples were cleaned, pulverized (<250 μm), and homogenized in individual cups. As the majority of the paleosols were noncalcic Alfisols, the acid pretreatment was excluded because the error associated with the chemical index of alteration minus potassium (CIA-K) proxy is minimal and falls within the error margin (Michel et al., 2022), and the paleosol-paleoclimate model (PPM) uses untreated soil composition (Stinchcomb et al., 2016). Samples were sent to ALS Chemex (Reno, Nevada) for bead fusion and X-ray fluorescence analysis of 13 major elements. Analytical uncertainty was maintained between 0.001% and 0.1% (depending on element analyzed; see Supplemental Data S1[1]), and duplicate analyses had a mean standard deviation <0.5%. Whole-rock major elements were then corrected for loss on ignition (LOI) and converted to molar masses before being used as inputs for standard paleosol weathering indices (e.g., CIA-K and paleosol weathering index [PWI]) and relevant climofunctions.

For reconstructing paleotemperatures, two methods were used to estimate mean annual temperature (MAT): the PWI and $PPM_{1.0}$. The PWI climofunction was described by Gallagher and Sheldon (2013) as:

$$\mathrm{MAT}(^{\circ}\mathrm{C}) = -2.74\ln(PWI) + 21.39; \mathrm{SE} = \pm 2.1^{\circ}\mathrm{C}. \quad (1)$$

$$PWI = 100\{(42\times Na) + (166\times Mg) + (5.54\times K) + (2.05\times Ca)\}. \quad (2)$$

This method was developed based on the relationship between MAT ($R^2 = 0.57$) and the relative loss of major cations from B horizons during chemical weathering and subsequent leaching, where SE is standard error. We limited this paleothermometer to paleosols having PWI <60, because PWI >60 would indicate paleosols that are not distinguishable from parent material (Gallagher and Sheldon, 2013). The $PPM_{1.0}$ model is an open-access data-driven spline regression model that includes 11 major and minor oxides and an expanded training dataset including the widest range of soils and climates of any of the described climofunctions, and it produced MAT values with a root mean squared prediction error (RMSPE) of ±4.0 °C (Stinchcomb et al., 2016).

Paleoprecipitation estimates were determined using the CIA-K value as an input for the mean annual precipitation (MAP) climofunction ($R^2 = 0.72$) of Sheldon et al. (2002):

$$\mathrm{MAP}(\mathrm{mm\ yr^{-1}}) = 221.1e^{0.0197(\mathrm{CIA-K})}; \mathrm{SE} = \pm 299\ \mathrm{mm\ yr^{-1}}. \quad (3)$$

$$\mathrm{CIA-K} = 100\times\frac{\mathrm{Al}}{(\mathrm{Al}+\mathrm{Ca}+\mathrm{Na})}. \quad (4)$$

This climofunction is based on the principle that silicate mineral weathering forms clay by hydrolysis and acid attack reactions; as moisture content controls these reactions, a wetter climate would promote clay formation (Sheldon et al.,

[1]Supplemental Material. Supplemental materials include a data file with raw data and a text file containing biomarker analysis interpretations along with exemplar phytolith figures. Please visit https://doi.org/10.1130/GSAB.S.28374089 to access the supplemental material; contact editing@geosociety.org with any questions.

2002). The error margin for MAP reconstruction based on CIA-K has been updated to reflect the dataset from Lukens et al. (2019), replacing the Marbut (1935) dataset previously used by Sheldon and Tabor (2009). The application of the CIA-K climofunction is restricted to noncalcic paleosols (Sheldon et al., 2002). Additionally, the $PPM_{1.0}$ model also uses its data-driven spline regression model to produce MAP estimates, with a root mean squared prediction error (RMSPE) of ±512 mm yr^{-1}.

3.3. Paleovegetation Reconstruction

Paleovegetation reconstructions were carried out using two different methods: phytolith assemblages and bulk carbon isotopic analysis of soil organic matter ($\delta^{13}C_{org}$). Samples for phytolith analysis were prepared following a modified version of the method presented by Strömberg (2003). In total, 28 samples were selected and analyzed for phytolith-based reconstructions from Angastaco and La Viña Basins. Briefly, the procedure included (1) taking a subsample of an A horizon paleosol (1–3 g) and crushing it into finer fragments, (2) subsequent sieving and oxidation of the fragments in Schultz's solution to remove the larger particles (>250 μm) and organic matter, (3) deflocculation and clay removal via fine sieves (53 μm) and deionized water washes, and (4) using $ZnBr_2$, a heavy liquid with a specific gravity of 2.3 g/cm^3, to float the phytoliths for separation from remaining grains. Phytoliths were placed on slides with Cargille Meltmount (R.I. = 1.539) and analyzed to identify different phytolith morphotypes; at least 300 grains per slide were documented for quantitative analysis, following Strömberg (2003). This procedure was carried out on a Nikon Eclipse N-E compound/petrographic microscope under high magnification (200–1000×) at North Carolina State University.

Identification of morphotypes was based on both fossil and modern reference collections (Strömberg, 2003, 2004; PhytCore DB, Albert et al., 2016; and E.G. Hyland's reference collections at North Carolina State University), and it followed the nomenclature and descriptors developed by the International Code for Phytolith Nomenclature (ICPN1.0, Madella et al., 2005; ICPN2.0, Neumann et al., 2019). Morphotypes were broadly grouped into two categories: forest indicators and grass (land) indicators (see Supplemental Figs. S7 and S8). Forest indicator morphotypes included Forest (FI), Dicotyledon (DICOT), Conifer (CONI), Conifer/Monocotyledon (CONI/MONO), Sedge (SEDGE), Palm (PALM), Bambusoid (BAMB), and Marantacea/Costaceae (MAR/COST). Grass indicator morphotypes were further used to estimate abundances for C_4 versus C_3 vegetation. Based on the morphotypes produced within the subclades of PACMAD (Panicoideae [PANI], Aristidoideae, Chloridoideae [CHLOR], Micrairioideae, Arundinoideae, Danthonioideae), maximum and minimum abundances of C_4 vegetation were estimated based on Strömberg and McInerney (2011) using the following formulae:

$$C_{4\ \text{maximum}} = \frac{\text{PACMAD} + \text{PANI} + \text{CHLOR}}{\text{GRASS} + \text{POOID} + \text{PACMAD} + \text{PANI} + \text{CHLOR}}. \quad (5)$$

$$C_{4\ \text{minimum}} = \frac{\text{PANI} + \text{CHLOR}}{\text{GRASS} + \text{POOID} + \text{PACMAD} + \text{PANI} + \text{CHLOR}}. \quad (6)$$

Pooid grasses (POOID).

Additionally, a bootstrapping function was used for error calculation, computing 95% confidence intervals (CIs) for estimating errors in the abundance of each functional plant type (Chen et al., 2015; Hyland et al., 2023).

Samples for bulk paleosol $\delta^{13}C_{org}$ analysis were collected from A horizons as described above. Seventeen samples from the Angastaco Basin and 12 samples from the La Viña Basin were processed for isotopic analysis. Samples were ultrasonicated in methanol to remove labile modern organic matter and reacted with 6% HCl to remove carbonates. Samples were rinsed with deionized water until they reached a neutral pH and dried overnight in an oven at 80 °C. Dry samples were homogenized and weighed into tin capsules, which were then loaded into the autosampler of a Costech Elemental Analyzer attached to a Delta V + isotope ratio mass spectrometer at either North Carolina State University's Paleo^3 Laboratory or California State University–Northridge's Stable Isotope Laboratory. The $\delta^{13}C_{org}$ values are expressed in per mil (‰) relative to the Vienna Peedee belemnite (VPDB) standard. Calibration was performed using U.S. Geological Survey (USGS) standards, including USGS61 ($\delta^{13}C = -35.05‰ \pm 0.04‰$), USGS62 ($\delta^{13}C = -14.79‰ \pm 0.04‰$), and USGS63 ($\delta^{13}C = -1.17‰ \pm 0.04‰$). Analytical uncertainty for $\delta^{13}C_{org}$ values was maintained at ~0.1‰, and average standard error for replicate analyses was 0.4‰.

To determine the abundance of C_3 and C_4 biomass from the $\delta^{13}C_{org}$ signatures, we constructed a two-component mixing model with C_3 and C_4 end members after the proposed model of Cotton et al. (2012, 2014). C_3 and C_4 plants display distinct isotopic signatures, with C_4 plants exhibiting enriched $\delta^{13}C_{org}$ values compared to C_3 plants. However, the isotopic composition varies due to climate conditions and atmospheric CO_2 concentration ($\delta^{13}C_{atm}$). Within modern ecosystems, the $\delta^{13}C_{org}$ values for C_3 plants span a broad range (−37‰ to −23‰), reflecting variations associated with humidity and plant taxonomy (e.g., Diefendorf et al., 2010; Sheldon et al., 2020). In addition, fluctuating $\delta^{13}C_{atm}$ compositions through time also cause $\delta^{13}C_{org}$ values to shift. Therefore, to determine cutoff and end-member values to estimate C_3 versus C_4 plant abundances during the late Miocene within our study sites, it was crucial to consider the $\delta^{13}C_{atm}$ estimates and climate conditions of the studied interval. We employed two different end-member mixing models to estimate maximum and minimum percentages of C_4 vegetation.

For the maximum C_4 vegetation estimate, we followed the Cotton et al. (2012, 2014) model, which uses corrections for local MAP regime and atmospheric composition ($\delta^{13}C_{atm}$) to adjust the end members for pure C_3 and C_4 vegetation. For determination of the C_3 end member based on precipitation and aridity, we used the modern plant database of Diefendorf et al. (2010), which compiles $\delta^{13}C_{org}$ values of modern C_3 plants growing across a wide range of MAP conditions. Based on our paleoclimate reconstruction (Section 3.2), the estimated MAP for Angastaco Basin (Palo Pintado Formation) ranged between 484 mm yr^{-1} and 1084 mm yr^{-1} (Section 4). Based on Diefendorf et al. (2010), the mean $\delta^{13}C_{org}$ value of C_3 plants growing between 500 mm yr^{-1} and 1000 mm yr^{-1} is −27.0‰. For the atmospheric $\delta^{13}C$ correction, we used the modern $\delta^{13}C_{atm}$ value of −8‰ and reconstructed the late Miocene (7.4–5.95 Ma) $\delta^{13}C_{atm}$ value of −6.4‰ from Tipple et al. (2010). Therefore, the estimated C_3 end-member value of $\delta^{13}C_{org}$ for Angastaco Basin was −25.4‰. C_4 plants lack a similar relationship between their isotopic composition and precipitation/aridity and are generally enriched (+14‰) relative to C_3 plants for a given atmospheric composition. Cotton et al. (2012) considered a slight correction of −0.3‰ based on Buchmann et al. (1996), resulting in a reconstructed end-member value of −11.7‰ for the mean $\delta^{13}C$ value of C_4 plants during our study period. For La Viña Basin, we followed a similar procedure, using a MAP range between 190 mm yr^{-1} and 1277 mm yr^{-1}, and determined the precipitation-based $\delta^{13}C_{org}$ value of −26.9‰ for modern C_3 plants from Diefendorf et al. (2010). After applying a correction based on Miocene $\delta^{13}C_{atm}$, we estimated the C_3 end-member values for the Huayquerian, Laventan, Friasian, and Santacrucian SALMA intervals at the La Viña Basin. The estimated C_3 end-member values for these intervals were −24.8‰, −24.8‰, −24.0‰, and −24.4‰, respectively.

We estimated C_4 end-member values for these intervals to be −11.1‰, −11.1‰, −10.3‰, and −10.7‰, respectively.

Our second end-member model used a conservative approach to determine minimum estimates of C_4 vegetation. Previous studies suggested values of $\delta^{13}C_{org}$ ranging from −24‰ to −22.3‰ as the most enriched possible C_3 values (Passey et al., 2009; Cotton et al., 2012, 2014). In line with the suggested values, we selected −22.3‰ as the most possible enriched value for C_3 plants based on the estimated MAP (Section 4), and, therefore, any value for $\delta^{13}C_{org}$ enriched more than −22.3‰ would indicate some input from C_4 vegetation. We estimated the maximum and minimum C_4 vegetation from both sites using these two end-member suites (see Supplemental Data S1).

3.4. Polycyclic Aromatic Hydrocarbons (PAHs)

Incomplete combustion and pyrolysis of organic matter result in the formation of polycyclic aromatic hydrocarbons (PAHs) that resist degradation and allow better preservation in soil compared to the traditionally used charcoal and pollen methods for reconstructing fire activity (Lau et al., 2010). Modern gas chromatograph analytical techniques were used to analyze PAH concentrations and reconstruct the paleofire regime for the study sites. For PAH analysis, bulk paleosol samples from A horizons were crushed into a fine powder (<62.5 μm), rinsed with acetone to remove modern contaminants, and left to dry. After crushing again, the samples were transferred to a glass fiber thimble and lowered into a Soxhlet apparatus, where a solution of 85:15 dichloromethane:acetone was used as a solvent. After running for 24 h, cycling 4–6 times per hour, the contents were transferred to a rotary evaporator flask, where the solvent mixture was evaporated. The sample was redissolved in dichloromethane and transferred to a gas chromatography (GC) vial, to which was added an internal standard mixture at a 1:20 ratio (v/v) of internal standard to sample. The internal standards were deuterated PAHs: naphthalene d-8, acenaphthene d-10, phenanthrene d-10, chrysene d-12, and perylene d-12. The samples were then analyzed using a Thermo Trace 1310 Gas Chromatograph equipped with an ISQ mass spectrometer detector at California State University–Northridge. Each run was preceded by nine calibration standards containing 63 compounds, and a test standard was run before each new GC sequence to verify instrument accuracy.

Samples were analyzed in Selective Ion Monitoring (SIM) mode to enhance the instrument's sensitivity for all compounds, including the 16 Environmental Protection Agency (EPA) PAHs and alkylated PAHs targeted for quantification. In addition to the EPA 16 PAHs, benzo(e) pyrene (BeP), perylene (PERY), retene (RET), dibenzofuran (DBF), dibenzothiophene (DBT), long-chain *n*-alkanes (C12-C38), and alkylated PAHs (C1-C4 NAP, C1-C4 ANT/PHE, C1 FLE, C1 FLU/PYR, and C1-C2 CHY/BaA) were also quantified. Standard quantification and confirmation ions were employed in SIM mode, with peak areas calculated relative to deuterated internal standards using both internal and external standards for quantification. For alkylated PAHs without specific standards, quantification was based on response factors of the closest available standard compound. The detection limit for PAHs in paleosols and soils was ∼0.1 μg/kg. Soxhlet extraction was used for all samples, with six duplicate samples and eight method blanks analyzed to ensure accuracy.

PAHs can originate from two primary sources: petrogenic and pyrogenic. Petrogenic PAHs are formed through slow geological processes, while pyrogenic PAHs are produced by the incomplete combustion of organic materials such as wood, fossil fuels, and vegetation. These PAHs can undergo weathering due to environmental exposure and burial, complicating paleoenvironmental and paleofire reconstructions. To differentiate between petrogenic and pyrogenic PAHs, the alkylated PAH derivative index (APDI; Karp et al., 2020) was utilized. To further distinguish between sources and isolate the pyrogenic component associated with vegetation combustion, a non-negative matrix factorization (NNMF) was applied to alkylated phenanthrenes (Karp et al., 2021b; Lee and Seung, 1999). Additionally, the low molecular weight (LMW) ratio from Karp et al. (2020) was employed to determine the depositional mechanisms for PAHs. To address preservation bias between samples, we normalized the total PAH concentrations using C31 alkane (Karp et al., 2020; Ghosh, 2021). Further details of these analyses are provided in the Supplemental Text.

To determine the fire input, we followed relationships described by Denis et al. (2017) and Karp et al. (2021a):

$$\text{Fire input} = \sum\left(\frac{\text{Pyrogenic PAH}}{\text{C}_{31}\text{ alkane}}\right). \quad (7)$$

The list of PAHs analyzed for total concentrations were as follows: phenanthrene (PHE), anthracene (ANT), fluoranthene (FLU), pyrene (PYR), RET, benz[a]anthracene (BaA), chrysene (CHY), benzo[k]fluoranthene (BkF), BeP, benzo[a]pyrene (BaP), indeno[1,2,3-cd]pyrene (IND), and benzo[ghi]perylene (BgP).

To determine vegetation burn provenance, we used a combination of the retene proxy (Ramdahl, 1983; Simoneit et al., 1993) and the DMP-x and DMP-y proxies (Simoneit and Mazurek, 1982; Kappenberg et al., 2019; Karp et al., 2020):

$$\text{Retene Proxy} = \frac{\text{Retene}}{\sum(\text{Pyrogenic PAH})}, \quad (8)$$

$$\text{DMP} - \text{x proxy} = \frac{\begin{matrix}1,7-\text{DMP}\\ +2,6\,|\,3,5-\text{DMP}\end{matrix}}{\begin{matrix}1,7-\text{DMP}+2,6\,|\,3,5\\ -\text{DMP}+1,2\\ -\text{DMP}\end{matrix}}, \quad (9)$$

$$\text{DMP} - \text{y proxy} = \frac{1,7-\text{DMP}}{1,2-\text{DMP}}, \quad (10)$$

where DMP stands for dimethylphenanthrene. A minimum value of 0 for the retene proxy indicates pyrogenic PAHs derived from an angiosperm-dominated ecosystem, while values approaching 1 indicate pyrogenic PAHs derived from gymnosperms. For the DMP-x proxy, values closer to 0 indicate pyrogenic PAHs derived from angiosperm trees, while values near 1 indicate pyrogenic PAHs derived from gymnosperms. Similarly, DMP-y values closer to 0 indicate angiosperm trees, while higher values (>10) indicate gymnosperms. Details of this method can be found in the Supplemental Text S2.

4. RESULTS

4.1. Angastaco Basin

The Palo Pintado Formation within the Angastaco Basin contains >1700 m of sediments, primarily composed of laminated mudrocks, trough cross-bedded sandstone, and coarse sandstone with pebbles and burrows (Fig. 3). The overall lithology and structures suggest two depositional settings for the Palo Pintado Formation The lower part (0–950 m) shows an abundance of pebbly, coarse sandstones and trough cross-laminated sand with minor laminated mudrocks (Fig. 3). The upper part (950–1760 m) shows a sudden increase in mudrocks and clast-supported conglomerates with decreased pebbly sands (Fig. 3). We also identified two ash beds: the first (A-1) at 8 m and the second (A-2) at 1730 m.

We identified 48 paleosols throughout the section. These were categorized into four pedotypes based on physical characteristics (Fig. 4) and included a Protosol/Inceptisol (AG-1), a Gleysol/Alfisol (AG-2), an Argillisol/Alfisol (AG-3), and a Gypsisol/Aridisol (AG-4) (e.g., Mack

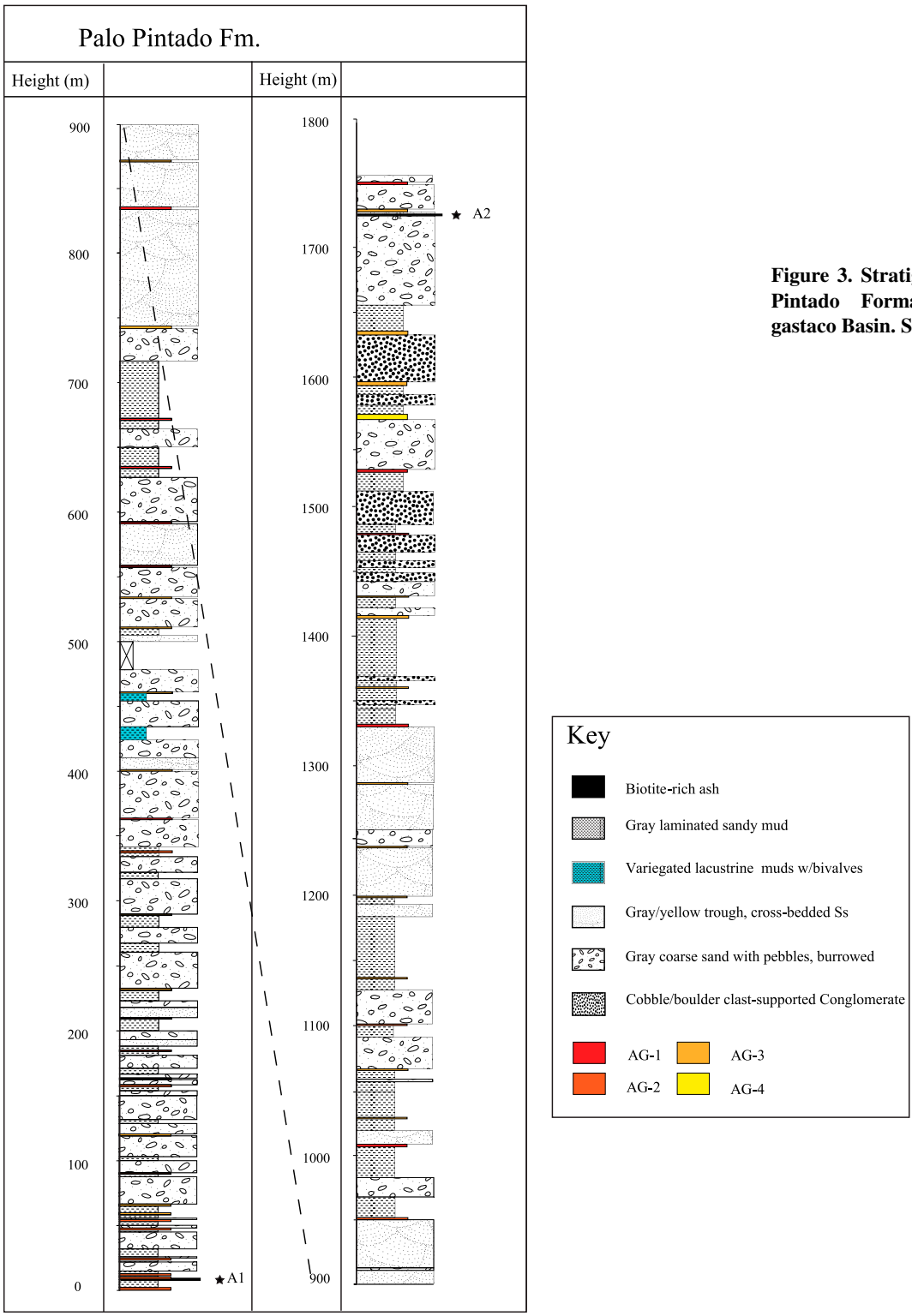

Figure 3. Stratigraphy of Palo Pintado Formation in Angastaco Basin. Ss—sandstone.

et al., 1993; Retallack, 2008; Soil Survey Staff, 2014; Fig. 4). AG-1 is a poorly developed soil that contains root traces and sand lenses within a gray sandy A horizon (<1 m thick) and lacks a B horizon. AG-2 is a moderately developed soil with a reddish silty A horizon (~1.5 m thick) with root traces, a distinct Bg horizon (gleying/mottles), and a brown silty C horizon (Fig. 4). AG-3, another moderately developed soil, has a purple, silty A horizon (>1 m thick) with root traces and burrows underlain by a Bt horizon with mottles and clay cutans (Fig. 4). AG-4 is a moderately developed soil with A, Bw, By, and C horizons; the A horizon (>1.5 m thick) is composed of brown sandy silt and has root traces, and the B and By horizons show light-green mottles and gypsum nodules, respectively (Fig. 4). Of these 48 paleosols, AG-2 and AG-3

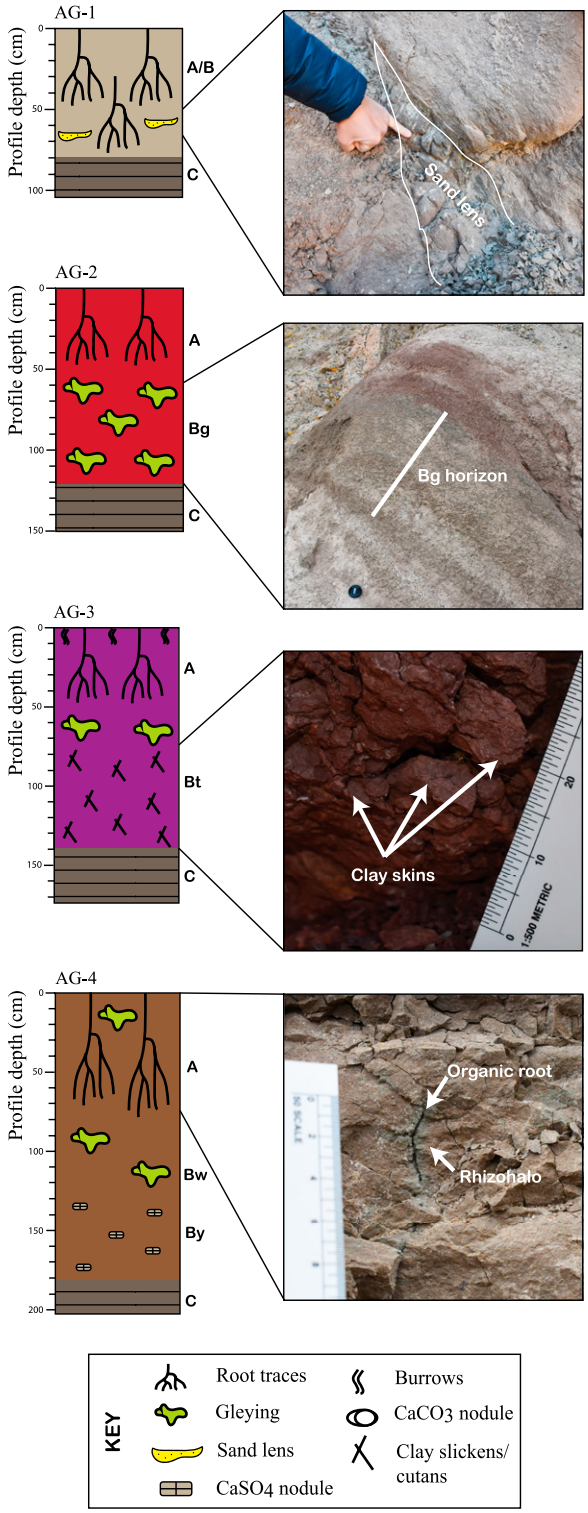

Figure 4. Pedotypes identified within the Palo Pintado Formation: AG-1—Protosol/Inceptisol, AG-2—Gleysol/Alfisol, AG-3—Argillisol/Alfisol, and AG-4—Gypsisol/Aridisol.

pedotypes are relatively common throughout the section (see Supplemental Data S1), while AG-1 and AG-4 are mostly restricted to specific intervals in the middle and upper parts of the formation (Fig. 3).

Paleotemperature estimates based on the PWI proxy showed that MAT varied between 10.2 °C and 10.9 ± 2.1 °C with an average of 10.5 °C (Fig. 5A). This reconstruction suggests very little to no change in MAT throughout the studied interval. PPM-based reconstructions revealed an average MAT of 10.4 °C that varied between 9.4 °C and 11.4 ± 4 °C (Fig. 5A). None of these reconstructions showed a significant trend, with all reconstructions within error of one another throughout the studied interval. Paleoprecipitation estimates from CIA-K ranged between 757 mm yr^{-1} and 1085 ± 299 mm yr^{-1} with an average of 912 mm yr^{-1} (Fig. 5B). Compared to this, the reconstruction based on $PPM_{1.0}$ suggested an average MAP of 747 mm yr^{-1}, ranging from 414 mm yr^{-1} to 1032 ± 512 mm yr^{-1} (Fig. 5B); overall, these methods are within error and suggest an overall decreasing trend in precipitation over the investigated interval. The geochemical compositions of the paleosol samples from the Angastaco Basin, including major- and minor-element percentages such as Ti/Al, are reported in the Supplemental Data S1.

We analyzed 19 biomarker samples from the Palo Pintado Formation, and, based on the NNMF analysis and APDI values, we identified mixed fractions of pyrogenic and petrogenic PAH signals (see Supplemental Text S2, Figs. S3–S6). While the APDI proxy suggested mixed pyrogenic and petrogenic sources for Palo Pintado samples, the ratio of methyl phenanthrene (MPh) to phenanthrene (Ph) showed only pyrogenic sources (MPh/Ph <2.43; Supplemental Data S1, Figs. S1 and S3). LMW ratios indicated that most of these PAH samples reflect residues of primary combustion (Supplemental Fig. S1). Comparison of the pyrogenic fraction of PAH burn input normalized over C_{31} alkane revealed an order of 60 magnitude increase in fire occurrence at ca. 7 Ma followed by a decline toward 6 Ma (Fig. 5C; see also Supplemental Data S1). Overall, there appears to be a directional decrease in pyrogenic PAH abundances, which we interpret as a decrease in fire occurrence over the investigated interval (Fig. 5C). We also used the retene, DMP-x, and DMP-y values to differentiate between the vegetation burn residue. The retene values ranged from 0.04 to 0.50 with an average of 0.22 ($\sigma = 0.13$), which suggests a mostly angiosperm-dominated ecosystem with some mixed angiosperm-gymnosperm mixed burn input (Supplemental Data S1). The DMP-y values from these samples varied between 0.58 and 11.59 with an average of 5.11 ($\sigma = 3$), while DMP-x values from this site varied between 0.52 and 1 with an average of 0.87 ($\sigma = 0.13$) (Figs. 6A and 6B). DMP-y and DMP-x values suggest gymnosperm dominance with minor angiosperm presence (Fig. 6B) within the studied interval. Neither of these proxies showed any directional trends through time.

The $\delta^{13}C_{org}$ values of 17 samples collected from the Palo Pintado Formation ranged from −30.2‰ to −23.5‰, with an average value of −26.0‰ (Fig. 6C; Supplemental Data S1). Based on our maximum estimates of C_4 abundance using the end member of −25.4‰ for C_3 (Section 3.3), a mixed signal of C_3-C_4 was iden-

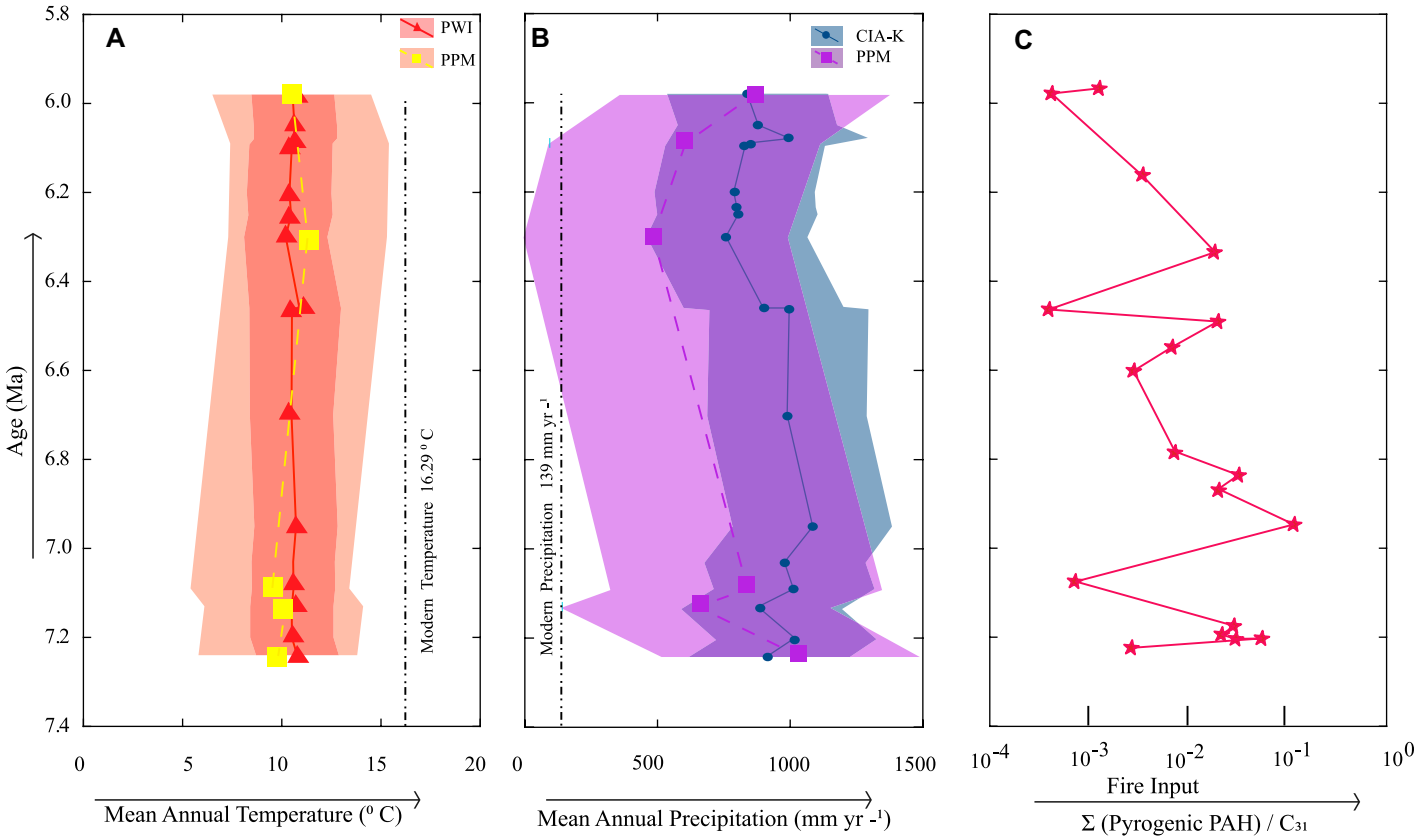

Figure 5. Paleoclimate and paleofire reconstructions from Palo Pintado: (A) mean annual temperature (MAT), where paleotemperature reconstructions are based on the paleosol weathering index (PWI; red triangles) and paleosol paleoclimate model ($PPM_{1.0}$; yellow squares); (B) mean annual precipitation (MAP), where paleoprecipitation reconstructions are based on chemical index of alteration minus potassium (CIA-K; blue circles) and paleosol paleoclimate model ($PPM_{1.0}$; purple squares); and (C) fire input based on polycyclic aromatic hydrocarbons (PAHs; red stars).

tified at ca. 6.8–6 Ma. The estimates of maximum C_4 vegetation range from 0% to 13.7% (Fig. 6C; Supplemental Data S1), with an average value of 2.2% ($\sigma = 3.7\%$). The minimum C_4 vegetation estimates based on a cutoff value of −22.3‰ for pure C_3 ecosystem show a lack of C_4 vegetation throughout the studied interval (Supplemental Data S1). Nineteen samples from Palo Pintado Formation were analyzed using phytolith analysis, with an average of 31 morphotypes (~77 submorphotypes) identified per slide and an average of 321 counts (see Supplemental Data S1). The analysis included identification and categorization of both diagnostic (D) and nondiagnostic (ND) morphotypes, including nondiagnostic compound variable groups such as POOID-ND, PALM-ND, GRASS/MONO-ND, and Other (OTH; see Section 3.3), and 14 diagnostic compound variable groups, including forest indicators (FI) and grass indicators (FI-GEN, DICOT-GEN, DICOT-WO, CONI/MONO, CONI, SEDGE, PALM-D, MAR/COST, BAMB/B, GRASS-D, POOID-D, PACMAD-GEN, and PANI [GEN—General; WO—Woody; B—Basal]). Phytolith assemblages suggested that the ecosystem in the Palo Pintado Formation was dominated by forests; the average estimated forest biomass was 52.5%, with significant but smaller input from grasses, comprising an average of 30.6% ($\sigma = 8\%$, range = 16% to 46%) of the total vegetation throughout the section (Fig. 6D; Supplemental Data S1). Based on the assemblages, the grasses were primarily composed of C_3 plants, with a minor proportion of C_4 plants in the upper section (Fig. 6D). C_4 vegetation estimates based on 19 phytolith samples ranged from a minimum value of 0%–18.2% (average = 2.5%, $\sigma = 4.7\%$) to a maximum value of 0%–21.8% (average = 3.3%, $\sigma = 5.6\%$). C_4 morphotypes were mostly equally distributed among CHLOR, PACMAD, and PANI, although some samples showed a dominance of one group over the other (see Supplemental Data S1). Paleovegetation estimates from phytolith assemblages agreed with $\delta^{13}C_{org}$-based reconstructions, with consistent minimum and maximum C_4 estimates.

4.2. La Viña Basin

La Viña Basin comprises ~650 m of sediments, mostly mudstone and cross-bedded sandstone. A 250-m-thick section of the Jesús María Formation was identified, characterized by laminated mud at the base and trough cross-bedded sandstone at the top (Fig. 7). It is overlain by a 250-m-thick, brown, laminated mudstone and trough cross-bedded sandstone and interbedded laminated evaporite identified as the Guanaco Formation (Fig. 7). The overlying 150-m-thick trough cross-bedded fine and medium sandstone interbedded with laminated mud is identified as the Piquete Formation. Four ash beds were identified within the Jesús María Formation at 1 m (A-1), 10 m (A-2), 19 m (A-3), and 129 m (A-4), with an additional ash bed (A-5) located within the Guanaco Formation at 412 m (Fig. 7).

Twenty-eight paleosols were identified, which were classified into four pedotypes (Fig. 8): Alfisol/Calcic Argillisol (LV-1), Alfisol/Argillisol (LV-2), Inceptisol/Gypsisol (LV-3), and Inceptisol/Protosol (LV-4) (e.g., Mack et al.,

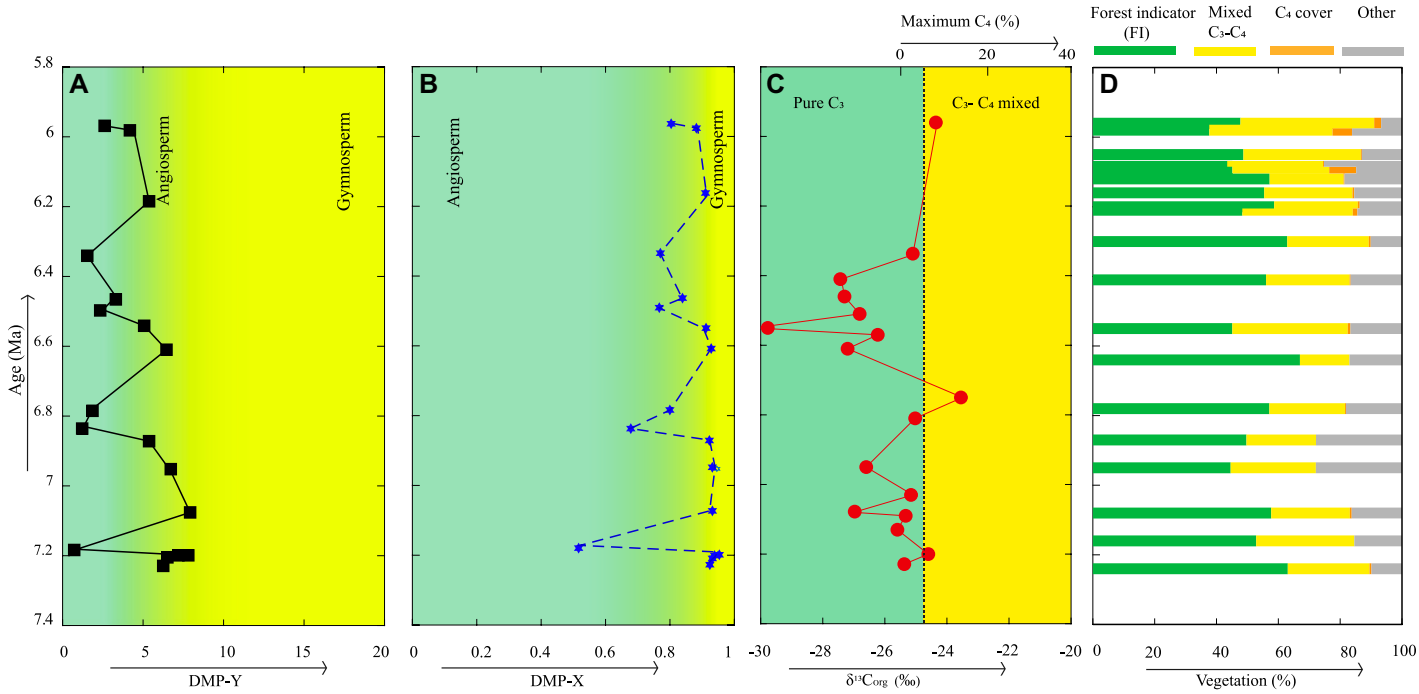

Figure 6. Paleovegetation reconstruction from Palo Pintado: (A) DMP-y; (B) DMP-x; (C) carbon isotope composition ($\delta^{13}C_{org}$) and maximum C_4 percentage (cutoff value, 25.5‰); and (D) phytolith-based paleovegetation composition. DMP—dimethylphenanthrene.

1993; Retallack, 2008; Soil Survey Staff, 2014). LV-1 is a moderately developed soil with an A horizon (orange silty sand, <1 m thick) showing root traces, a Bw horizon with mottling and clay cutans, a Bk horizon with calcium carbonate nodules, and a C horizon (Fig. 8). It is common in both the Jesús María and Guanaco Formations. LV-2 consists of three horizons: A, Bt, and C (Fig. 8), where the A horizon is >1 m thick and is composed of dark-red silt with visible root traces and mottling, and the Bt horizon contains abundant clay cutans and rare iron nodules. LV-2 is primarily restricted to the Jesús María Formation. LV-3 is a moderately developed soil with A, By, and C horizons, where the A horizon contains root traces and mottling, while the By horizon contains abundant gypsum nodules (Fig. 8). Within the studied section, only two paleosols of this pedotype were identified, one within the Jesús María Formation at 75 m and the other in the Guanaco Formation at 90 m. LV-4 is a poorly developed paleosol with an A/B horizon showing some light root traces, light-green mottling, and sand lenses (Fig. 8). It was predominantly found within the Guanaco Formation. The Piquete Formation, which unconformably overlies the Guanaco Formation, did not contain any identified paleosol horizons and therefore was not included in the paleoclimate and paleovegetation reconstructions.

We analyzed six samples of paleosol matrix from the Jesús María Formation and five from the Guanaco Formation for paleoclimatic reconstructions. Paleotemperature reconstructions with the PWI proxy showed that MAT varied between 9.4 °C and 10.9 ± 2.1 °C within the Jesús María Formation and between 8.4 °C and 10.9 ± 2.1 °C within the Guanaco Formation (Fig. 9A). The average MAT was calculated to be 10.1 °C for the entire interval. In addition, PPM estimates suggested an average MAT of 11.1 °C, which varied between 8.5 °C and 15.7 ± 4 °C (Fig. 9A). None of these reconstructions revealed any significant temperature change within the studied section in La Viña Basin, and all proxies were in agreement within error. Paleoprecipitation estimates (CIA-K) for the Jesús María Formation varied between 557 mm yr^{-1} and 1101 ± 299 mm yr^{-1}, with an average of 881 mm yr^{-1} (Fig. 9B). For the Guanaco Formation, MAP estimates ranged between 324 mm yr^{-1} and 954 ± 299 mm yr^{-1}, with an average of 748 mm yr^{-1}. These paleoprecipitation estimates suggest that the Guanaco Formation had slightly drier conditions compared to the underlying Jesús María Formation, a trend that was also observed in the $PPM_{1.0}$ reconstructions (Fig. 9B). $PPM_{1.0}$ estimates suggested that MAP varied between 934 mm yr^{-1} and 1277 ± 512 mm yr^{-1}, averaging 1105 mm yr^{-1} for the Jesús María Formation. However, for the Guanaco Formation, the average dropped to 441 mm yr^{-1} with a range between 190 mm yr^{-1} and 655 ± 512 mm yr^{-1} (see Supplemental Data S1). While PPM reconstructions were slightly lower than CIA-K values, both indicated a significant drop in MAP throughout this interval. The geochemical compositions of the paleosol samples from the La Viña Basin, including major- and minor-element percentages such as Ti/Al, are reported in the Supplemental Data S1.

Thirteen samples from the La Viña Basin were analyzed for PAHs. Based on the NNMF analysis, we identified mixed fractions of pyrogenic and petrogenic PAH signals (see Supplemental Figs S5 and S6). Both the APDI proxy and ratio of MPh to Ph agreed and showed pyrogenic sources for these samples (MPh/Ph <2.43; see Supplemental Material Data S1, Figs. S2 and S5). Based on the LMW ratio, most of the PAH signals were identified as in-place combustion residue, except for two samples, at 12 Ma and 8 Ma, which indicated smoke-derived PAHs (see Supplemental Data S1). The comparison of the pyrogenic fraction of PAH burn inputs showed a wide variability in fire contributions, with no discernible trend observed (see Supplemental Data S1). Overall, there does not appear to be a directional trend in fire input over the investigated interval (Fig. 9C). The ratio of retene and PAHs varied between 0.03 and 0.50 with an average of 0.13 ($\sigma = 0.12$) and suggests a mostly angiosperm-dominated ecosystem during the investigated interval (see Supplemental Data S1). DMP-y values varied between 1.65 and 16.15 with an average of 6.69 ($\sigma = 3.41$) (Fig. 10A),

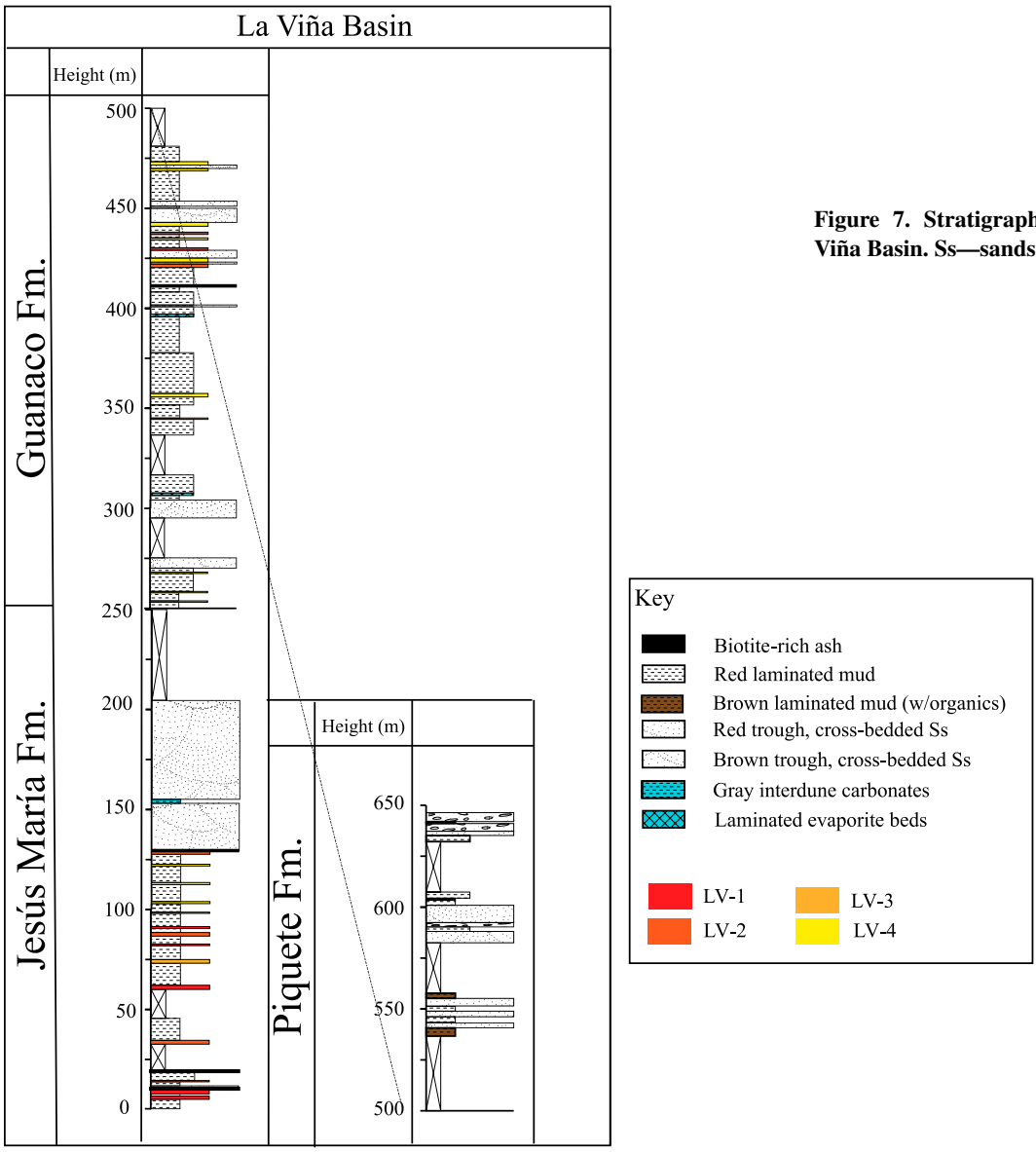

Figure 7. Stratigraphy of La Viña Basin. Ss—sandstone.

and DMP-x values ranged between 0.69 and 1 with an average of 0.93 ($\sigma = 0.07$) (Fig. 10B). These values suggest a gymnosperm-dominated ecosystem with two intervals of enhanced angiosperms ca. 12 Ma and 8 Ma (Figs. 10A and 10B).

The $\delta^{13}C_{org}$ values from 12 samples from La Viña Basin varied between −25.7‰ and −20.3‰ with an average of −24.1‰. There appears to be a directional trend toward more enriched values over the investigated interval (Fig. 10C). Based on the maximum C_4 estimates from carbon isotopes for the Huayquerian, Laventan, Friasian, and Santacrucian (Section 3.3), we identified the first mixed ecosystem (C_3-C_4) within the Jesús María Formation at 15.5 Ma, with additional occurrences in the Guanaco Formation toward the upper section ca. 8 Ma (Fig. 10C). Our mixing model suggests that through time, the ecosystem was initially C_3-dominated and then transitioned to a mixed C_3-C_4 system by the end of the section. The maximum C_4 vegetation estimates based on the mixing model vary between 0% and 32.6% with an average of 6.5% ($\sigma = 10.7\%$; Fig. 10C; Supplemental Data S1), while the minimum C_4 estimates vary between 0% and 14.6% (average = 1.7%; $\sigma = 4.2\%$; see Supplemental Data S1). These estimates show an increase in C_4 vegetation (~15%) in the upper Guanaco Formation.

Phytolith assemblages were counted for paleovegetation reconstruction as well. We analyzed nine slides from La Viña Basin and identified 27 morphotypes (~66 submorphotypes) with an average of 338 counts per slide. Similar to Angastaco Basin, we categorized both diagnostic and nondiagnostic morphotypes. Twelve diagnostic compound variable groups were identified. Nine forest indicators (FI) included FI-GEN, DICOT-GEN, DICOT-WO, CONI/MONO, CONI, SEDGE, PALM-D, MAR/COST, and BAMB/B (see Section 3.3). The remaining four were grass indicators (GI): GRASS-D, POOID-D, PACMAD-GEN, and PANI (see Section 3.3). The nondiagnostic groups were POOID-ND, PALM-ND, GRASS/MONO-ND, and OTH. Phytolith analysis showed that the FI morphotypes comprised most of the assemblage; on average, we estimated that 71% of the biomass in the area was from forest vegetation, whereas grassland vegetation accounted for an average of 18% ($\sigma = 2\%$; range = 21%–14%; Fig. 10D). Estimates for C_4 vegetation at La Viña Basin ranged from a minimum value of 0%–6.5% (average = 2.2%;

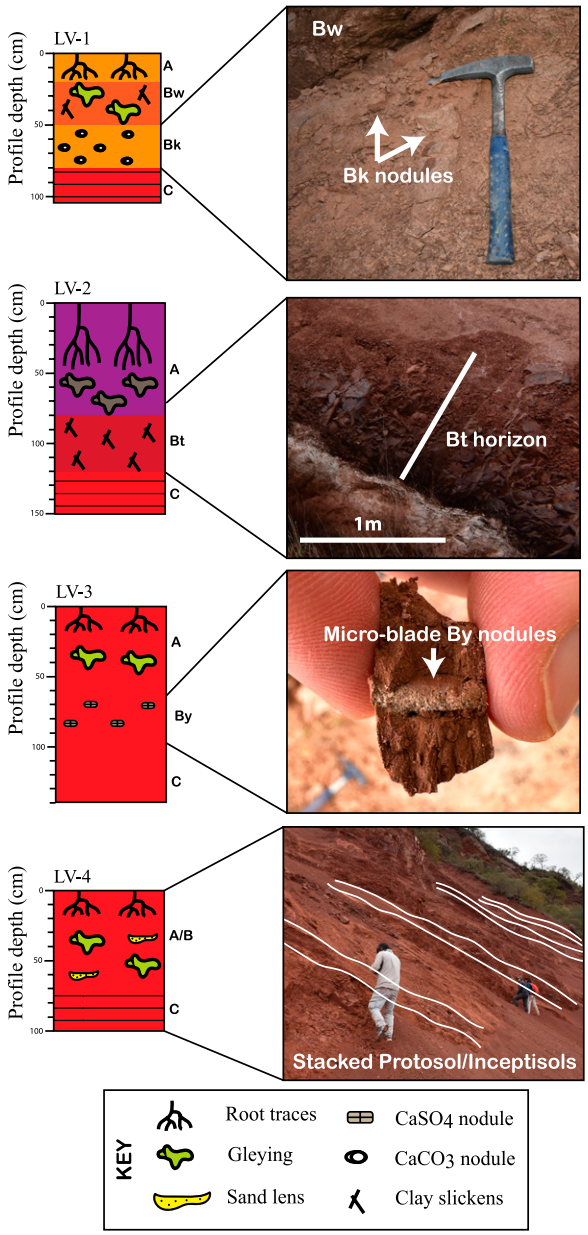

Figure 8. Pedotypes identified within the La Viña Basin: LV-1—Alfisol/Calcic Argillisol, LV-2—Alfisol/Argillisol, LV-3—Inceptisol/Gypsisol, and LV-4—Inceptisol/Protosol.

$\sigma = 2\%$) to maximum values of 0%–8.5% (average = 3.2%; $\sigma = 3.2\%$) (see Supplemental Data S1). C_4 morphotypes in this section included PANI and PACMAD; CHLOR indicators were absent. Paleovegetation estimates from phytolith assemblages differed from those derived from $\delta^{13}C_{org}$, with $\delta^{13}C_{org}$ indicating a higher presence of C_4 vegetation than phytoliths.

5. DISCUSSION

5.1. Stratigraphy, Facies, and Paleosols

The Jesús María Formation (ca. 17–12 Ma) reveals two distinct units. The lower portion is composed of thick, red, laminated mud reflecting a low-energy depositional setting along with several well-developed paleosol horizons consistent with a lacustrine deposit that experienced periodic subaerial exposure (Scherer et al., 2007, 2015). The lower portion is overlain by a thick trough cross-bedded sandstone with interdune carbonate, signifying relatively higher depositional energy associated with a fluvial environment (Miall, 2014). The overlying Guanaco Formation (ca. 12–7.48 Ma) indicates a fluctuation in depositional energy associated with a fluviolacustrine setting where the trough cross-bedded sandstone represents a fluvial environment (Miall, 2014) while the laminated mud with evaporite beds represent a lacustrine environment (Scherer et al., 2015). The youngest Piquete Formation (ca. 6.2–4.08 Ma), characterized by laminated mud and trough cross-bedded sandstone with rip-up clasts and burrows, reflects sediment reworking. The facies association suggests a floodplain deposit (Scherer et al., 2015).

The coeval Palo Pintado Formation (ca. 7.24–5.96 Ma) contains a thick accumulation of sediment recording a variable depositional environment. A thick, gray, coarse sand with pebbles and alternating laminated sandy mud and trough cross-bedded sandstone occupying the lower ~950 m indicate a relatively higher-energy fluvial setting (Miall, 2014). The lateral migration of sand bars indicated by trough cross-bedded sand, with overbank fines such as mudstone and multiple paleosol horizons, points toward a meandering fluvial depositional environment. The upper ~800 m interval is composed of clast-supported conglomerate with coarse, pebbly sand and indicates a fluvial setting with high energy. The coarser and thicker nature of the deposit, along with the development of paleosol horizons, suggest a braided river depositional environment (Miall, 2014). The mud facies indicate overbank deposits, and the coarser sand and conglomerate deposit, with trough cross-bedding, are associated with channel deposits (Scherer et al., 2007).

These interpretations agree with previous studies that suggest an ephemeral fluvial setting for the Jesús María Formation within the Angastaco Basin (Starck and Anzótegui, 2001), while the overlying Guanaco and Piquete Formations indicate a more permanently established fluvial system with variable depositional energy (Carrapa et al., 2012). Alternatively, these formations could represent a fluvial system associated with an alluvial fan developed in the distal zone (Galli et al., 2023). The transition indicates the role of tectonics in basin rearrangement, impacting the local hydrology. This becomes more evident in the Palo Pintado Formation, which was deposited in a meandering fluvial system and is suggested to record multiple episodes of tectonic reactivation, leading to the formation of an intermontane basin (Galli et al., 2017; Ulberich et al., 2021). Tectonic processes controlling the basin evolution and configuration were accompanied by changes in climate patterns (Starck and Anzótegui, 2001).

Paleosol types identified in this study can be broadly classified into four categories represented throughout both sections, though their distribution is not proportional and constant. The most common paleosol type in both areas is the Inceptisol/Protosol (AG-1, LV-4), characterized by minimal development and a lack of distinct sedimentary features that differentiate them from Entisols. They are commonly identified within fluvial or high-energy depositional

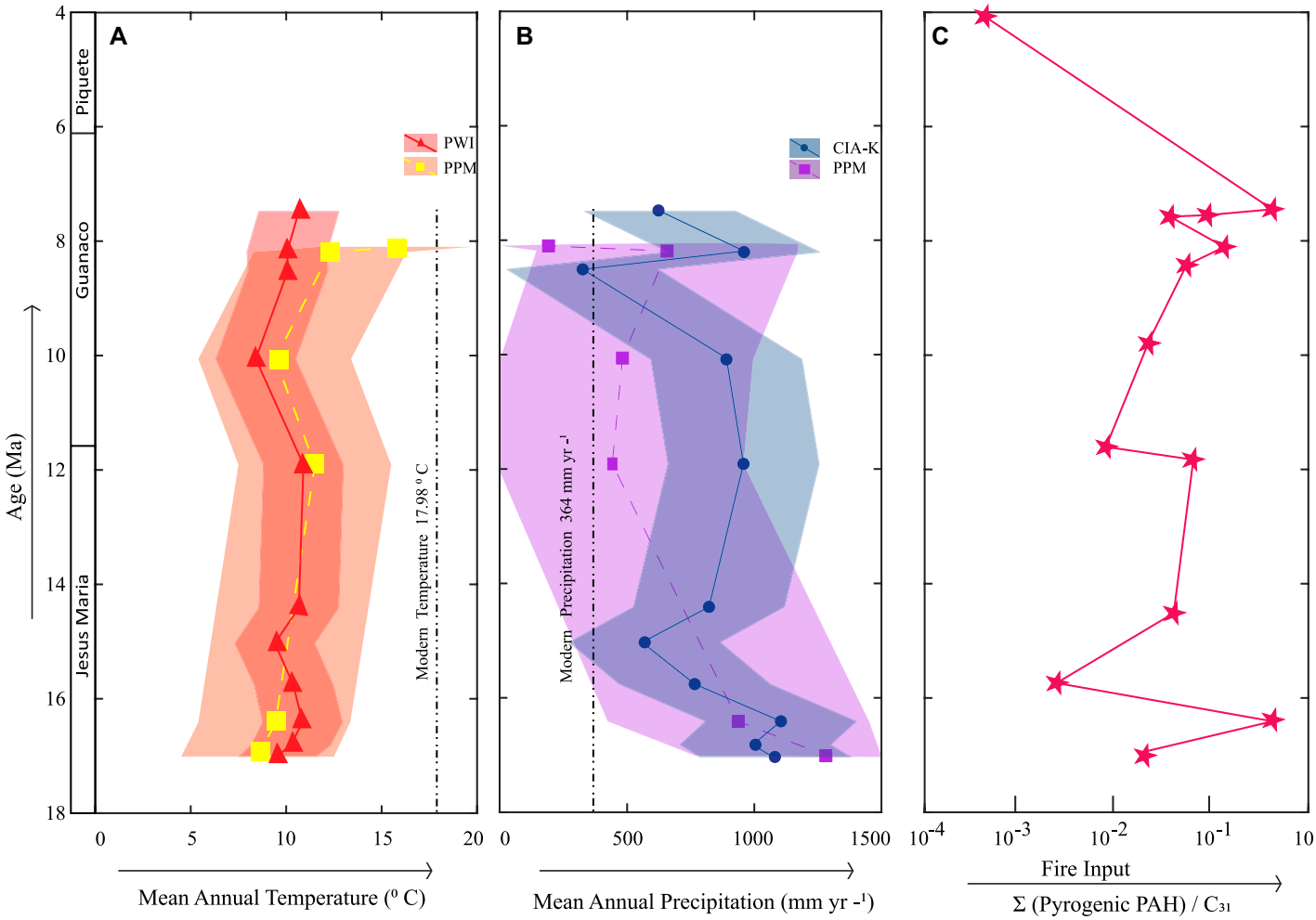

Figure 9. Paleoclimate reconstructions from La Viña Basin: (A) mean annual temperature (MAT), where paleotemperature reconstructions are based on the paleosol weathering index (PWI; red triangles) and paleosol paleoclimate model ($PPM_{1.0}$; yellow squares); (B) mean annual precipitation (MAP), where paleoprecipitation reconstructions are based on chemical index of alteration minus potassium (CIA-K; blue circles) and paleosol paleoclimate model ($PPM_{1.0}$; purple squares); and (C) fire input based on polycyclic aromatic hydrocarbons (PAHs; red stars).

settings (Figs. 3 and 7), indicating their proximity to fluvial distributary systems (Sheldon and Tabor, 2009), as evidenced by sand lenses. Alfisol/Argillisol (Ag-2, Ag-3, and Ag-4 and LV-1 and 2) paleosols, defined by moderate development with root traces, cutans, and mottling/gleying, are also common throughout the studied interval. The clayey accumulations and ped structures in well-defined B horizons suggest a longer period of soil development. Cutans on surfaces are indicative of illuviation and can result from clay shrinkage and swelling from intermittent water infiltration and evaporation, while mottling indicates recurrent waterlogging, signifying localized decomposition and organic material reduction (Retallack, 1988, 1994). Occurrences of calcite (calcic Alfisol, LV-1) and/or gypsum (Gypsisol, AG-4) nodules are noted in some paleosols as well, which indicate a seasonally or variably dry climate that promoted the growth of calcium/gypsum nodules in the vadose zone (Breecker et al., 2009; Retallack, 2005). These are accompanied by the evaporite beds in the upper Jesús María and Guanaco Formations (Fig. 7).

The frequent presence of similar paleosols in both sites indicates a connection between the environmental conditions at these locations and their relationship to the depositional settings. Paleosol morphology and chemical composition data allow the reconstruction of paleoenvironmental conditions. The presence of cutans and the existence of gypsum and carbonate nodules in both sites indicate the development of some paleosols under variable or evolving moisture conditions, which in some cases may be indicative of seasonal climates (Retallack, 2005; Hatano and Yoshida, 2017). The Ti/Al ratio is a reliable provenance indicator as it remains primarily unaffected by diagenetic processes (Sheldon, 2006; Stiles and Stensvold, 2008). Ti/Al from Palo Pintado and La Viña remains relatively constant with an average value of ~0.05 for both sites (Supplemental Data S1). Relatively low values (<0.1) with minimal changes in Ti/Al suggest similar parental materials and weathering intensity (Sheldon and Tabor, 2009) and allow for quantitative reconstruction and comparison of paleoclimate from these localities.

One important caveat in paleosol analysis is the postburial and diagenetic alteration that can impose secondary signals, complicating further climate and environmental inferences (Sheldon and Tabor, 2009; Hyland and Sheldon, 2013). While it is common for paleosols to undergo some level of compaction, no evidence of extreme burial compaction has been noted

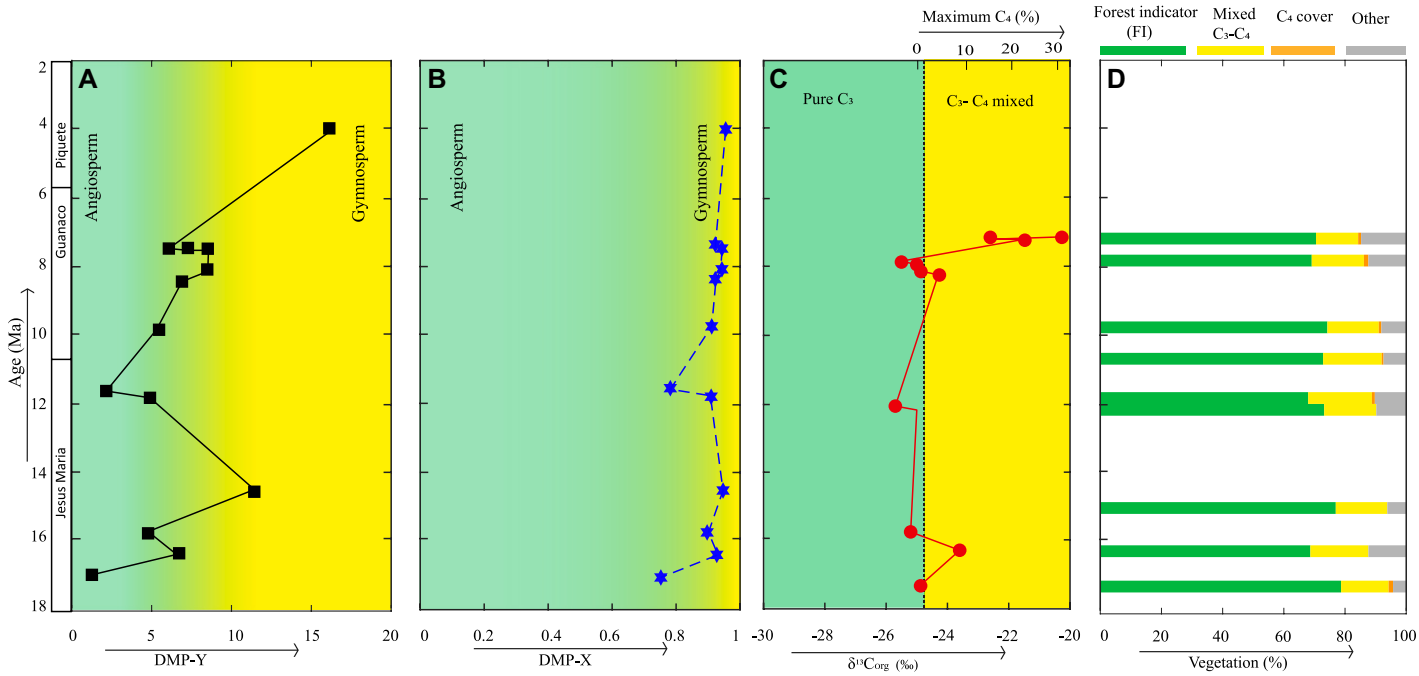

Figure 10. Paleovegetation reconstruction from La Viña Basin: (A) DMP-y; (B) DMP-x; (C) carbon isotope composition ($\delta^{13}C_{org}$) and maximum C_4 percentage (cutoff value, 24‰); and (D) phytolith-based paleovegetation composition. DMP—dimethylphenanthrene.

within the studied paleosol horizons, and burial depths here are considered minimal (e.g., Carrapa et al., 2012). Secondary weathering and diagenetic alterations can also complicate the paleosol analysis and reconstructions (Michel et al., 2016; Retallack, 1991). Except for one occurrence of reprecipitated gypsum in the Guanaco Formation (between 55 m and 65 m), no other evidence of secondary mineral precipitations has been identified. CIA-K values estimated from the elemental ratios of the geochemical compositions of Bt horizons also show little variation throughout, suggesting consistency in the weathering regime. Therefore, the identified paleosol horizons remain useful for further climate and environmental analysis applications.

5.2. Paleoclimate Reconstructions

Paleotemperature reconstructions in La Viña and Angastaco Basins lack any significant changes through time. Our multiproxy estimates suggest an average annual temperature of ~10 °C in Angastaco Basin and ~11 °C in La Viña Basin. The $PPM_{1.0}$-based estimates follow a similar pattern as the paleosol weathering index reconstructions (Figs. 4A and 7A). While there is a general agreement among the estimated temperatures, these values indicate substantially cooler conditions than modern values (~16 °C; Fick and Hijmans, 2017). These proxies may be a better indicator of temperature trends than of absolute values (Hyland and Sheldon, 2016) but regardless suggest that temperature was not a driving factor in any environmental shifts across this interval. Late Miocene paleorecords indicate that the global climate was warmer than present, with atmospheric CO_2 concentrations ranging between 200 ppm and 400 ppm (Bradshaw et al., 2012; Carrapa et al., 2019; Steinthorsdottir et al., 2021). The average temperature in South America during the late Miocene was similar to pre-industrial values, except for regions experiencing active orogenic processes (Bradshaw et al., 2012).

In contrast to temperature, precipitation patterns in the late Miocene were considerably different from those in the modern day. The onset of precipitation seasonality has been identified around the late Miocene in South America (Mulch et al., 2010), gradually transitioning to modern conditions. Paleoprecipitation reconstructions from Angastaco and La Viña Basins suggest fluctuations between subarid and subhumid conditions. At Angastaco Basin, estimated MAP averages 912 mm yr^{-1} using CIA-K and 747 mm yr^{-1} based on $PPM_{1.0}$. Both reconstructions are generally within error and suggest an overall decrease in MAP over the studied interval (Fig. 5B) with consistently wetter conditions than the modern conditions (~139 mm yr^{-1}). At La Viña Basin, these same proxies estimate 821 mm yr^{-1} (CIA-K) and 662 mm yr^{-1} ($PPM_{1.0}$) (Fig. 9B), which also indicate wetter conditions than modern conditions (364 mm yr^{-1}). While reconstructions from both basins are within error of each other, $PPM_{1.0}$-based values are consistently lower as compared to CIA-K estimates. It should be noted that the uncertainties associated with the $PPM_{1.0}$-based estimates are higher than those reported for CIA-K, but the reason for these consistently lower estimates is unclear. While the absolute values of the reconstructions might be over- or underestimated depending on the proxy reconstruction method, the general trend is still valid to denote the changes in the climatic conditions, with decreased precipitation through time.

During the late Miocene, global climate and hydrological conditions exhibited regional variability, with some areas experiencing enhanced precipitation while others underwent drying. Global events such as the closure of the Tethys gateway and the Central American Seaway, and major orogens in central and southeastern Asia, eastern North America, the central Andes, and the European Alps impacted regional and global climate (Steinthorsdottir et al., 2021). While subtropical regions experienced increased aridity, parts of Europe, Asia, and the Americas saw enhanced seasonality and precipitation patterns (Griffin, 2002; Dupont et al., 2013; Herbert et al., 2016). Paleoprecipitation records indicate persistently wetter conditions in southwest Europe, contrasted by aridification trends in central Europe during the late Miocene (Böhme et al., 2008). Enhanced seasonality and intensification of several monsoon systems are important features of the Miocene. The Asian mon-

soon system, established by the late Miocene, intensified due to the Himalayan orogeny and Tibetan Plateau uplift, leading to aridification in inner Asia and increased precipitation in southern and southeastern Asia (Spicer, 2017; Clift and Webb, 2019). Griffin (2002) suggested that the development of the Asian monsoon system interacted with the Mediterranean and resulted in progressive aridification in North Africa during the late Miocene. The development of the Asian monsoon system thus gave rise to zones of intense precipitation and aridification, a trend observed in South America as well.

Carrapa et al. (2019) suggested a link between late Miocene aridification in South America and global climate changes that influenced the Hadley cell circulation. The strengthening of the Hadley circulation during this period enhanced moisture convergence toward the Intertropical Convergence Zone (ITCZ), while the subtropics experienced greater moisture divergence, reinforcing aridification in the region. The SASM system introduced regional changes in precipitation patterns linked to the Andean orogeny, enhancing precipitation on the eastern flank and promoting aridification on the western flank (Bookhagen and Strecker, 2008). A broader shift toward increased rainfall has been noted in previous studies (Starck and Anzótegui, 2001; Pingel et al., 2016; Rohrmann et al., 2016); however, the Angastaco and La Viña Basins in NW Argentina record progressive aridification (Figs. 5 and 9; e.g., Carrapa et al., 2011). The tectonic deformation progressing eastward and the late Miocene uplift of local mountain ranges surrounding and splitting the retroarc foreland basin (into the Angastaco and La Viña Basins) likely contributed significantly to this aridification (Hain et al., 2011; Galli et al., 2023).

The orogenic adjustments occurring around the Angastaco and La Viña Basins might have induced a local rain-shadow effect, consequently contributing to the drying climate observed in the area. Our comprehensive paleoclimate reconstruction records do suggest a reduction in precipitation (Figs. 5B and 9B), indicative of local aridification during the latest Miocene (by ca. 6 Ma). However, the similarity in magnitude and timing of the aridification observed in both the Angastaco and La Viña Basins suggests a regional influence rather than solely local topographic changes associated with features such as the Sierra de los Colorados, Cerro Negro, or Cumbre de Luracatao (cf. Carrapa et al., 2012).

5.3. Paleovegetation Records and Comparisons

Paleovegetation reconstructions from the La Viña and Angastaco Basins indicate that forest-dominated ecosystems with mixed grasses/shrubs persisted during ca. 17–5 Ma based on the bulk carbon isotope signatures, phytolith assemblages, and PAHs. Our paleovegetation reconstructions identified the first appearance of C_4 vegetation ca. 16.4 Ma (phytolith) and 15.5 Ma ($\delta^{13}C_{org} = -23.6‰$), and the overall trends of the carbon isotopic signatures from both basins mark a moderate increase in C_4 percentage (to ~15% based on minimum C_4 estimates from $\delta^{13}C_{org}$; see Section 4.2) during the late Miocene (ca. 7 Ma; Figs. 6C and 10C). A similar trend was identified from the phytolith assemblages (Figs. 6D and 10D). Both isotope compositions and phytolith assemblages show a moderate increase in C_4 grasses, where carbon isotope–based reconstructions indicate a maximum peak of 32.5% C_4 at 7.5 Ma, contrasting with the maximum C_4 vegetation of 21% at 6.1 Ma shown through phytolith assemblages. Despite the similarity of the temporal variation in C_4 vegetation, a slight disparity in the absolute values of C_4 vegetation was observed between the carbon isotopic composition and phytolith assemblage records.

This difference may arise from either an underestimation based on phytolith assemblages or an overestimation based on carbon isotopic composition. Fredlund and Tieszen (1994) demonstrated that in the temperate ecosystem of the North American Great Plains, phytolith assemblages tend to underrepresent tall C_4 grasses (Panicoideae) and are counterbalanced by the overrepresentation of C_4 short grasses (Chlorideae), resulting in roughly accurate total % C_4. Additionally, grasses are known for being prolific producers of phytoliths (Hyland and Sheldon, 2013); therefore, it is unlikely that the phytolith assemblages would lead to an underestimation of C_4 grasses (see Section 3.3). Alternatively, uncertainties introduced by the isotopic reconstruction method might have resulted in the overestimation of C_4 grasses.

The estimate of maximum C_4 abundances from $\delta^{13}C_{org}$ values is controlled by several factors affecting carbon fractionation and soil organic carbon (SOC) preservation. During microbial decomposition of SOC, heterotrophic respiration of CO_2 preferentially respires ^{12}C, resulting in solid decomposition products enriched in ^{13}C by up to ~6‰ (Wynn, 2007), which might lead to overestimation of C_4 vegetation. Studies from modern soils show that the range of ^{13}C enrichment varies with climate and soil maturity (Krull et al., 2002; Krull and Bray, 2005) and suggest that preserved root materials can enrich $\delta^{13}C_{org}$ values by 2‰ and 2.3‰ for trees and forbs, respectively (Krull and Bray, 2005).

In addition, the overestimation could be attributed to the limitations imposed by the end-member values used in the isotope-based paleovegetation reconstruction. Our end-member values are based on Diefendorf et al. (2010), which investigated the correlation between carbon isotopes of leaves and MAP. Despite the comprehensive range of leaf $\delta^{13}C$ values in Diefendorf et al. (2010), there is a lack of data from South America. While several studies have demonstrated increased $\delta^{13}C_{org}$ values at higher altitudes due to temperature variation (Li et al., 2009) and atmospheric pressure (Zhou et al., 2013), Sheldon et al. (2020) found no strong correlation between $\delta^{13}C_{leaf}$ and elevation in gymnosperms. Regardless of the impact of altitude on isotopic discrimination, an expanded dataset from South America would help to address these discrepancies effectively.

Our minimum C_4 estimates, based on a more conservative cutoff value (−22.3%), underestimate C_4 vegetation compared to those reconstructed from phytolith assemblages (see Supplemental Data S1). While the absolute values of maximum/minimum C_4 estimates derived from $\delta^{13}C_{org}$ values do not precisely align with those obtained from the phytolith-based method, the overall trends agree. Both approaches indicate a predominance of C_3 vegetation over C_4 throughout the studied interval and identify an increase in C_4 cover by ca. 6 Ma in this area.

Our biomarker analysis also broadly agreed with these reconstructions. While the retene, DMP-x, and DMP-y values cannot be used to differentiate between C_3 versus C_4 cover specifically, we used these values to distinguish between gymnosperm and angiosperm groups and identify a broad trend in vegetation dynamics. However, we found discrepancies between the DMP-x and DMP-y values and retene values. Both the DMP-x and DMP-y values indicated a trend toward a gymnosperm-rich cover for the Palo Pintado Formation and La Viña Basin throughout the studied interval with minor angiosperm input at ca. 12 Ma, 8 Ma, and 7 Ma, while retene values denoted an absence/low abundance of gymnosperms throughout the studied interval (see Supplemental Data S1). Heppenheimer et al. (1992) suggested that diagenetic conditions such as temperature and pressure can cause alteration of retene to 1,7-DMP, thus increasing the DMP-x and DMP-y values (higher gymnosperm) and reducing the retene ratio, leading to a lower gymnosperm abundance based on the retene proxy. Such alteration can explain the disagreement between retene and DMP-x and DMP-y values observed here. However, NNMF analysis indicated pyrogenic sources for most of the samples, except for a minor petrogenic input, as evidenced by the APDI proxy for a few samples from the Palo Pintado Formation (Supplemental Material Data S1). Consider-

ing our multiproxy vegetation reconstruction holistically, these data collectively point toward a forest/woodland ecosystem with substantial presence of grasses (>20%) and with a lack of substantial C_4 cover (<10%) before ca. 8 Ma.

Previous studies have suggested a late Miocene transition from a forested ecosystem to a mosaic habitat with increasing grass vegetation in NW Argentina (Starck and Anzótegui, 2001; Zimicz et al., 2018; Ercoli et al., 2019). MacFadden et al. (1996) reported a transition from a C_3 ecosystem toward a mixed ecosystem with a significant component of C_4 grasses, which aligns with Latorre et al.'s (1997) findings of C_4 enrichment in the late Miocene based on soil carbonates in NW Argentina. Specifically, in the Angastaco Basin, the Palo Pintado Formation has been proposed to represent a C_3 montane ecosystem based on mammal fossil assemblages (Candela et al., 2021) and isotopic values from pedogenic carbonates (Bywater-Reyes et al., 2010). However, Bywater-Reyes et al. (2010) identified $\delta^{13}C$ enrichment in the upper Palo Pintado Formation, though it remained inconclusive whether this enrichment was due to C_4 vegetation or aridity-induced stress. Our multiproxy reconstruction aligns with this $\delta^{13}C$ enrichment pattern, detecting the presence of C_4 vegetation through C_4 morphotypes (PANI, CHLOR) and $\delta^{13}C_{org}$ enrichment, with a gradual increase observed toward the end of our study interval (ca. 6 Ma). Our paleovegetation reconstruction suggests an increasing presence of grass, indicating a transition from a predominantly forested ecosystem to one with expanding grass vegetation and confirming the onset of C_4 presence in the late Miocene.

While significant increases in C_4 grasses in the late Miocene have been reported from different continents (e.g., Cerling et al., 1997; Latrubesse et al., 2010; Hyland et al., 2019; Feakins et al., 2020), regional variability in the timing and abundance of the C_4 vegetation is noted in South America. Latorre et al. (1997) presented enriched $\delta^{13}C$ values from paleosol carbonates from Puerta de Corral Quemado (PCQ in Fig. 11) in NW Argentina, suggesting the presence of C_4 vegetation during 7.3–6.7 Ma. Fossilized rodent teeth enamel data corroborate the presence of C_4 vegetation (Hynek et al., 2012). However, using paleodiet as a paleovegetation proxy can lead to an overestimation of C_4 abundance due to dietary preferences (Cotton et al., 2014). Contrary to the previously suggested expansion of C_4 grasses (Kleinert and Strecker, 2001), Cotton et al. (2014) noted a lack of C_4 vegetation in Entre Rios, located farther south than Angastaco Basin (ER in Fig. 11). Instead, they reported a rise of C_3 grasses outcompeting palms and woodland vegetation in a cool, arid climate. Ghosh (2021) similarly observed the absence of C_4 grasses in Río Iruya, located farther north than Angastaco Basin (RI in Fig. 11). Their study suggested that a forest-dominated ecosystem persisted throughout the late Miocene, with the first appearance of C_4 grass noted at 6.6 Ma, though it remained in low abundances throughout the late Miocene. Findings from these studies and our records collectively show no evidence supporting a substantial C_4 expansion in NW Argentina during the late Miocene (Fig. 11). Instead, our reconstruction suggests a forest- or woodland-dominated ecosystem with minimal presence of C_4 grasses, similar to Rio Iruya and Entre Rios. Although we did not detect a substantial expansion of C_4 vegetation in the Angastaco/La Viña Basins, our study did still show a minor increase in C_4 abundance by the late Miocene (ca. 6 Ma). The expansion of C_4 vegetation (to modern abundances; cf. Powell and Still, 2009; Luo et al., 2024) in this region likely occurred slightly later than previously proposed (e.g., Latorre et al., 1997), perhaps during the Pliocene or Quaternary.

5.4. Drivers of C_4 Grasses and Possible Complications

Several mechanisms have been proposed to explain the late Miocene C_4 grass expansion, including declining atmospheric pCO_2 (e.g., Cerling et al., 1993). While the initial suggestion of declining atmospheric CO_2 concentrations seems unlikely, as CO_2 reconstructions suggest that concentrations fell below the threshold level (500 ppm) during the Oligocene and remained stable throughout the late Miocene (Pagani et al., 1999), this may have allowed for regionally different mechanisms to control the roughly contemporaneous phenomena on different continents. Aridification has been proposed as a driver of late Miocene C_4 grassland expansion in North America (Hyland et al., 2019), Africa (Sepulchre et al., 2006), and Asia (Huang et al., 2007). Prolonged aridity, along with corresponding increases in fire activity (e.g., Scheiter et al., 2012; Hoetzel et al., 2013; Bond, 2015), has been suggested as the cause of C_4 expansion in Africa (Dupont et al., 2013), the Tibetan Plateau (Hui et al., 2021), and the Indian subcontinent (Karp et al., 2021a). Additional studies from Asia and North America suggest the development of seasonal climates favored the expansion of C_4 grasses (Huang et al., 2007; Cotton et al., 2016).

The environmental shift toward aridity provides C_4 grasses with advantages over C_3 species (particularly trees and shrubs) due to the specialized adaptations of the C_4 photosynthetic pathway, including enhanced drought tolerance and high water-use efficiency (Christin and Osborne, 2014). We observed a slight increase in C_4 vegetation cover at our studied basins, coinciding with a decrease in precipitation, implying a relationship between vegetation and climate. Specifically, in the La Viña Basin, declines in MAP were recorded at 15 Ma and 8 Ma, aligning with the emergence and growth of C_4 vegetation. Similarly, ca. 6 Ma, a decreasing trend in MAP is correlated with expansion of C_4 vegetation, indicating a connection between local hydroclimate and vegetation dynamics. A transition to an arid climate with a stable warm temperature in the studied area might explain the increase in C_4 composition in this region, as C_4 plants have high water-use efficiency and drought tolerance (Christin and Osborne, 2014).

Fire clears out dense forest vegetation and promotes the growth of C_4 grasses by allowing more resources to be directed toward them, resulting in a positive fire-C_4 feedback loop. For example, Karp et al. (2018) identified an increased fire input in the Shivalik foothills of South Asia concurrent with increasing $\delta^{13}C_{org}$ values, indicating C_4 expansion. However, our PAH reconstruction of paleofire occurrences from La Viña Basin lacks any significant trend, and our records show a weak decline in fire input in the Angastaco Basin by the late Miocene. Similarly, Ghosh (2021) demonstrated that fire input does not correspond to the expansion of C_4 vegetation at a contemporaneous site farther north in Argentina. The absence of clear evidence for fire activity across the region implies a relatively limited role for fire in the expansion of C_4 vegetation, potentially because tree cover remained high, and the extent of C_4 cover at these sites might not have been substantial enough to trigger open-grassland feedback mechanisms (cf. Karp et al., 2018).

The development of seasonal climates has been proposed as a way to facilitate C_4 vegetation expansion, particularly in regions influenced by monsoon systems. Seasonal climates, characterized by alternating hot-wet and dry-cool seasons, create favorable conditions for C_4 grasses to thrive at the expense of forests (Osborne, 2008). Modern ecosystem studies support this notion, suggesting that increased warm-season precipitation promotes the dominance of C_4 vegetation over C_3 plants (Cabido et al., 2008). This relationship is also evident in the Miocene vegetation record, where late Miocene C_4 expansion was associated with elevated warm-season rainfall in East Asia (Huang et al., 2007), North America (Cotton et al., 2016), and Africa (Feakins, 2013). Though sparse, both proxy and model-based paleoclimate data suggest a change in the overall precipitation regime across this region during the late Miocene (Kleinert and

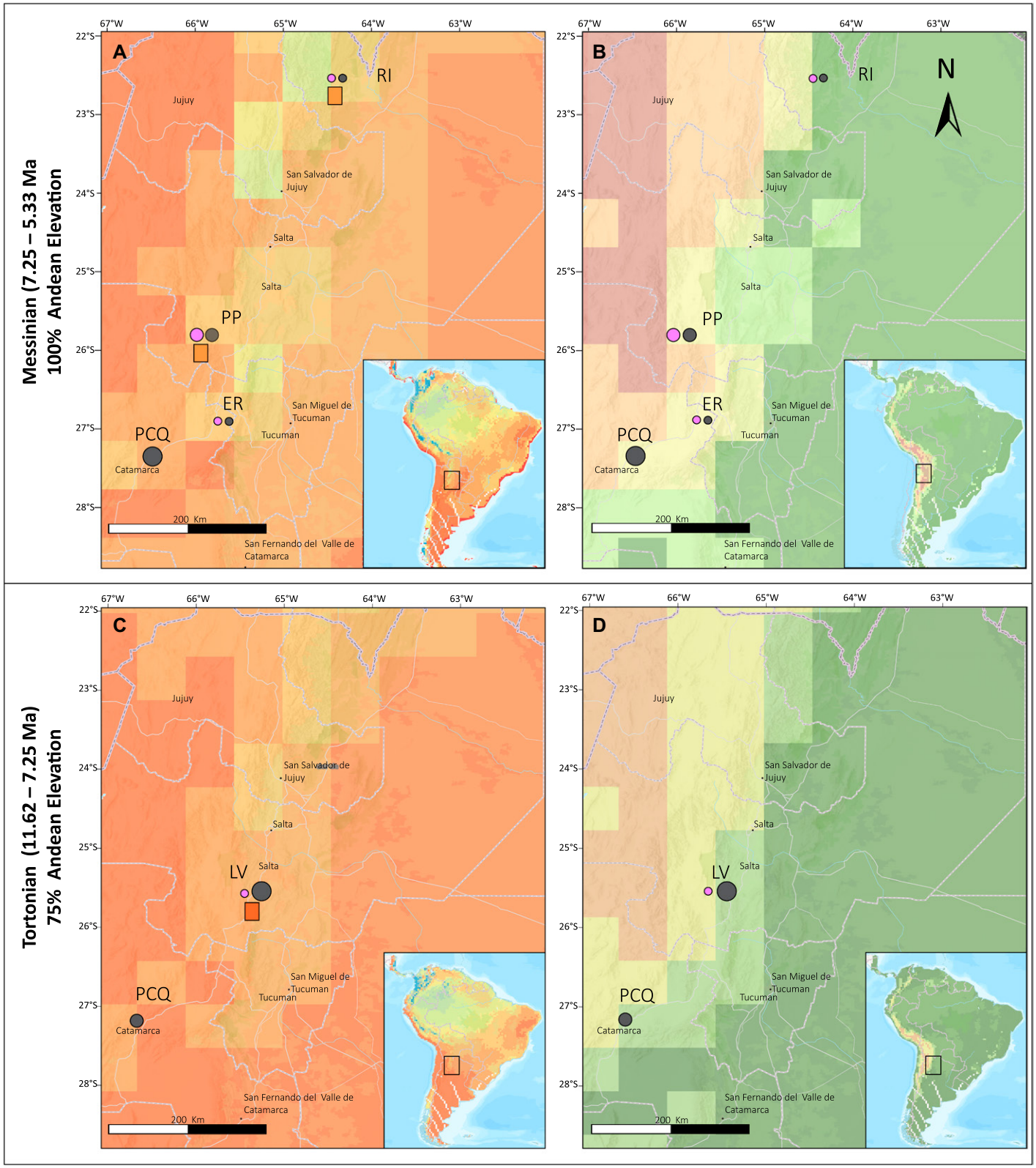

Figure 11. (A–D) Spatiotemporal variability in precipitation, $\delta^{13}C_{org}$ values, and C_4 vegetation signals during the Messinian (A, B) and Tortonian (C, D) in NW Argentina. Background map shows mean annual precipitation (A, C) for Andean elevation of 100% (B) and 75% (D) of modern elevation, respectively (after Insel et al., 2010). Acronyms, showing the locations of the proxy-derived mean annual precipitation (MAP) and C_4 vegetation estimates, are as follows: ER—Entre Rios; RI—Rio Iruya; PCQ—Puerta Corral Quemado; LV—La Viña; PP—Palo Pintado. Black polygon in insets indicates study area.

Strecker, 2001; Cotton et al., 2014; Carrapa et al., 2019; Candela et al., 2021; Tineo et al., 2022a, 2022b), and this change is linked with the development of seasonality (Starck and Anzótegui, 2001). This climatic shift is consistent with the development of an orographic barrier, which was in place once the Andes reached 50% of their modern elevation (Insel et al., 2010). Studies suggest that the Andes reached ~70% of their modern elevation by ca. 8 Ma and approached modern elevations by the late Miocene to Pliocene (Mulch et al., 2010; Insel et al., 2012). Therefore, the broader regional climate became a wetter, likely seasonal climate by the late Miocene, resulting in increased precipitation along the eastern flank of the Andes. At the same time, new structural ranges might have caused rain-shadow effects that caused drier conditions within the Angastaco and/or La Viña Basins. While our data do not preclude the possibility of a seasonal climate, the lack of direct evidence for seasonal variation highlights the need for further studies to provide more definitive proof and to clarify the extent of seasonality in the late Miocene climate of the region.

Regional vegetation dynamics seem to show a slight increase in C_4 vegetation during the Messinian (7.24–5.33 Ma; Fig. 11A) relative to the Tortonian (11.6–7.24 Ma; Fig. 11C), reflecting a potential correlation with this modeled shift in seasonality. Puerta Corral Quemado (PCQ; Latorre et al., 1997) and Palo Pintado (PP in Fig. 11C) show higher abundances in C_4 vegetation than Entre Ríos (ER; Cotton et al., 2014) and Río Iruya (RI; Ghosh, 2021) during the Messinian (Fig. 11A), while La Viña Basin shows higher abundances of C_4 vegetation by the Tortonian (Fig. 11C). Limited proxy support for this seasonality connection includes the abundance of PANI phytolith morphologies and the relative absence of CHLOR phytolith morphologies in the youngest portion of our record (see Supplemental Data S1), which have been linked to enhanced seasonality/monsoonal intensity in other regions (e.g., Kumar et al., 2022), indicating that a similar combined aridification/seasonality mechanism might have driven C_4 abundance in NW Argentina.

While we found a close relationship between declining precipitation and increased C_4 signals, neither of these proxies showed a rise in C_4 composition to high (>50%) levels as observed elsewhere during the late Miocene (e.g., Cerling et al., 1997; Fox and Koch, 2003; Hynek et al., 2012). Multiple factors control the distribution of C_4 grasses in the modern world, including temperature, precipitation, and elevation (e.g., Ehleringer et al., 1991; Edwards et al., 2010). In NW Argentina, elevation places a maximum limit on C_4 distributions by controlling local temperature and precipitation gradients (Tieszen et al., 1979; Cavagnaro, 1988; Cabido et al., 1997). These studies have shown that higher elevation favors C_3 grasses over C_4 grasses. Cavagnaro (1988) reported that in NW Argentina, the transition range for C_3-C_4 dominance is between 1100 m and 1600 m, above which C_3 grasses form the major component of the total vegetation. To investigate the impact of elevation, we compared the regional paleovegetation record against modeled elevation (Insel et al., 2010) during the Messinian (Fig. 11B) and Tortonian (Fig. 11D). During the Tortonian period, these sites likely were situated at elevations above 1000 m (Fig. 11B). Subsequently, they experienced uplift, consistently maintaining a high altitude throughout the late Miocene (Fig. 11D) as they approached their modern elevations. While our comparison suggests no direct correlation between C_4 abundance and elevation (Fig. 11), the already high elevation of these sites may have limited the maximum abundance of C_4 vegetation during the late Miocene, possibly explaining smaller or absent C_4 expansions observed in this and other elevated regions.

6. CONCLUSIONS

Here, we examined the link between paleoclimate and C_4 vegetation during the late Miocene in the Angastaco and La Viña Basins of NW Argentina. We reconstructed paleoclimate, paleofire, and paleovegetation conditions using a multiproxy approach from preserved paleosols within the Palo Pintado, Jesús María, and Guanaco Formations. The $\delta^{13}C_{org}$, biomarker (PAH), and phytolith assemblages suggest a forest/woodland-dominated ecosystem with low C_4 abundances. Paleosol geochemistry proxies show stable MAT and a gradual decline in MAP, leading to the onset of regional aridity. PAHs show an absence of a positive fire feedback mechanism during the late Miocene. Given the synchroneity in observed shifts in regional hydroclimate patterns and vegetation records, the minor increase in C_4 vegetation (ca. 8–6 Ma) appears to be correlated with aridification and possibly enhanced seasonality in NW Argentina. This suggests that the evolution of the SASM may have contributed to expanding C_4 grasslands in the region, but local elevation also likely provided a top-down control on maximum C_4 abundance. Further investigation is required to validate this hypothesis, necessitating the development of more robust climate-tectonic models coupled with proxy-based estimates that can directly reconstruct seasonal precipitation variations.

ACKNOWLEDGMENTS

We would like to thank the Servicio Geológico Minero Argentino (SEGEMAR), the National Scientific and Technical Research Council of Argentina (CONICET), and our collaborators for their assistance with fieldwork in Argentina. We also gratefully acknowledge the National Science Foundation for funding this research (grants 1854209 [to E.G. Hyland] and 1854404 [to J.M. Cotton]).

REFERENCES CITED

Albert, R.M., Ruíz, J.A., and Sans, A., 2016, PhytCore ODB: A new tool to improve efficiency in the management and exchange of information on phytoliths: Journal of Archaeological Science, v. 68, p. 98–105, https://doi.org/10.1016/j.jas.2015.10.014.

Andermann, T., Strömberg, C.A., Antonelli, A., and Silvestro, D., 2022, The origin and evolution of open habitats in North America inferred by Bayesian deep learning models: Nature Communications, v. 13, no. 1, 4833, https://doi.org/10.1038/s41467-022-32300-5.

Andrae, J.W., McInerney, F.A., Polissar, P.J., Sniderman, J.M.K., Howard, S., Hall, P.A., and Phelps, S.R., 2018, Initial expansion of C4 vegetation in Australia during the late Pliocene: Geophysical Research Letters, v. 45, no. 10, p. 4831–4840, https://doi.org/10.1029/2018GL077833.

Balcerak, E., 2011, Reconciling late Miocene climate and carbon dioxide levels: Eos, v. 92, no. 50, p. 476–476, https://doi.org/10.1029/2011EO500013.

Beerling, D.J., and Royer, D.L., 2011, Convergent Cenozoic CO2 history: Nature Geoscience, v. 4, no. 7, p. 418–420, https://doi.org/10.1038/ngeo1186.

Böhme, M., Ilg, A., and Winklhofer, M., 2008, Late Miocene "washhouse" climate in Europe: Earth and Planetary Science Letters, v. 275, no. 3–4, p. 393–401, https://doi.org/10.1016/j.epsl.2008.09.011.

Bond, W.J., 2015, Fires in the Cenozoic: A late flowering of flammable ecosystems: Frontiers in Plant Science, v. 5, p. 749, https://doi.org/10.3389/fpls.2014.00749.

Bond, W.J., Midgley, G.F., and Woodward, F.I., 2003, What controls South African vegetation—Climate or fire?: South African Journal of Botany, v. 69, no. 1, p. 79–91, https://doi.org/10.1016/S0254-6299(15)30362-8.

Bookhagen, B., and Strecker, M.R., 2008, Orographic barriers, high-resolution TRMM rainfall, and relief variations along the eastern Andes: Geophysical Research Letters, v. 35, no. 6, L06403, https://doi.org/10.1029/2007GL032011.

Bradshaw, C.D., Lunt, D.J., Flecker, R., Salzmann, U., Pound, M.J., Haywood, A.M., and Eronen, J.T., 2012, The relative roles of CO2 and palaeogeography in

determining late Miocene climate: Results from a terrestrial model–data comparison: Climate of the Past, v. 8, no. 4, p. 1257–1285, https://doi.org/10.5194/cp-8-1257-2012.

Breecker, D.O., Sharp, Z.D., and McFadden, L.D., 2009, Seasonal bias in the formation and stable isotopic composition of pedogenic carbonate in modern soils from central New Mexico, USA: Geological Society of America Bulletin, v. 121, no. 3–4, p. 630–640, https://doi.org/10.1130/B26413.1.

Buchmann, N., Brooks, J.R., Rapp, K.D., and Ehleringer, J.R., 1996, Carbon isotope composition of C4 grasses is influenced by light and water supply: Plant, Cell & Environment, v. 19, no. 4, p. 392–402, https://doi.org/10.1111/j.1365-3040.1996.tb00331.x.

Bywater-Reyes, S., Carrapa, B., Clementz, M., and Schoenbohm, L., 2010, Effect of late Cenozoic aridification on sedimentation in the Eastern Cordillera of northwest Argentina (Angastaco Basin): Geology, v. 38, no. 3, p. 235–238, https://doi.org/10.1130/G30532.1.

Cabido, M., Ateca, N., Astegiano, M., and Anton, A., 1997, Distribution of C3 and C4 grasses along an altitudinal gradient in central Argentina: Journal of Biogeography, v. 24, no. 2, p. 197–204, https://doi.org/10.1046/j.1365-2699.1997.00085.x.

Cabido, M., Pons, E., Cantero, J.J., Lewis, J.P., and Anton, A., 2008, Photosynthetic pathway variation among C4 grasses along a precipitation gradient in Argentina: Journal of Biogeography, v. 35, no. 1, p. 131–140, https://doi.org/10.1111/j.1365-2699.2007.01760.x.

Candela, A.M., Galli, C.I., Rasia, L.L., Voglino, D., Abello, M.A., Esponda, C.G., and Zurita, A.E., 2021, Late Miocene mammals from the Calchaquí Valley (Palo Pintado Formation, northwestern Argentina): Biogeographic and paleoenvironmental implications for the southern central Andes: Journal of South American Earth Sciences, v. 112, https://doi.org/10.1016/j.jsames.2021.103602.

Carrapa, B., Trimble, J.D., and Stockli, D.F., 2011, Patterns and timing of exhumation and deformation in the Eastern Cordillera of NW Argentina revealed by (U-Th)/He thermochronology: Tectonics, v. 30, no. 3, TC3003, https://doi.org/10.1029/2010TC002707.

Carrapa, B., Bywater-Reyes, S., DeCelles, P.G., Mortimer, E., and Gehrels, G.E., 2012, Late Eocene–Pliocene basin evolution in the Eastern Cordillera of northwestern Argentina (25°–26°S): Regional implications for Andean orogenic wedge development: Basin Research, v. 24, no. 3, p. 249–268, https://doi.org/10.1111/j.1365-2117.2011.00519.x.

Carrapa, B., Clementz, M., and Feng, R., 2019, Ecological and hydroclimate responses to strengthening of the Hadley circulation in South America during the late Miocene cooling: Proceedings of the National Academy of Sciences of the United States of America, v. 116, no. 20, p. 9747–9752, https://doi.org/10.1073/pnas.1810721116.

Cavagnaro, J.B., 1988, Distribution of C3 and C4 grasses at different altitudes in a temperate arid region of Argentina: Oecologia, v. 76, no. 2, p. 273–277, https://doi.org/10.1007/BF00379962.

Cerling, T.E., Wang, Y., and Quade, J., 1993, Expansion of C4 ecosystems as an indicator of global ecological change in the late Miocene: Nature, v. 361, no. 6410, p. 344–345, https://doi.org/10.1038/361344a0.

Cerling, T.E., Harris, J.M., MacFadden, B.J., Leakey, M.G., Quade, J., Eisenmann, V., and Ehleringer, J.R., 1997, Global vegetation change through the Miocene/Pliocene boundary: Nature, v. 389, no. 6647, p. 153–158, https://doi.org/10.1038/38229.

Chase, C.G., Sussman, A.J., and Coblentz, D.D., 2009, Curved Andes: Geoid, forebulge, and flexure: Lithosphere, v. 1, no. 6, p. 358–363, https://doi.org/10.1130/L67.1.

Chen, S.T., Smith, S.Y., Sheldon, N.D., and Strömberg, C.A., 2015, Regional-scale variability in the spread of grasslands in the late Miocene: Palaeogeography, Palaeoclimatology, Palaeoecology, v. 437, p. 42–52, https://doi.org/10.1016/j.palaeo.2015.07.020.

Christin, P.A., and Osborne, C.P., 2014, The evolutionary ecology of C4 plants: The New Phytologist, v. 204, no. 4, p. 765–781, https://doi.org/10.1111/nph.13033.

Christin, P.A., Edwards, E.J., Besnard, G., Boxall, S.F., Gregory, R., Kellogg, E.A., Hartwell, J., and Osborne, C.P., 2012, Adaptive evolution of C4 photosynthesis through recurrent lateral gene transfer: Current Biology, v. 22, no. 5, p. 445–449, https://doi.org/10.1016/j.cub.2012.01.054.

Clift, P.D., and Webb, A.A.G., 2019, A history of the Asian monsoon and its interactions with solid Earth tectonics in Cenozoic South Asia, *in* Treloar, P.J., and Searle, M.P., eds., Himalayan Tectonics: A Modern Synthesis: Geological Society, London, Special Publication 483, p. 631–652, https://doi.org/10.1144/SP483.1.

Cotton, J.M., Sheldon, N.D., and Strömberg, C.A., 2012, High-resolution isotopic record of C4 photosynthesis in a Miocene grassland: Palaeogeography, Palaeoclimatology, Palaeoecology, v. 337–338, p. 88–98, https://doi.org/10.1016/j.palaeo.2012.03.035.

Cotton, J.M., Hyland, E.G., and Sheldon, N.D., 2014, Multiproxy evidence for tectonic control on the expansion of C4 grasses in northwest Argentina: Earth and Planetary Science Letters, v. 395, p. 41–50, https://doi.org/10.1016/j.epsl.2014.03.014.

Cotton, J.M., Cerling, T.E., Hoppe, K.A., Mosier, T.M., and Still, C.J., 2016, Climate, CO2, and the history of North American grasses since the Last Glacial Maximum: Science Advances, v. 2, no. 3, https://doi.org/10.1126/sciadv.1501346.

Coutand, I., Carrapa, B., Deeken, A., Schmitt, A.K., Sobel, E.R., and Strecker, M.R., 2006, Propagation of orographic barriers along an active range front: Insights from sandstone petrography and detrital apatite fission-track thermochronology in the intramontane Angastaco Basin, NW Argentina: Basin Research, v. 18, no. 1, p. 1–26, https://doi.org/10.1111/j.1365-2117.2006.00283.x.

D'Antonio, C.M., and Vitousek, P.M., 1992, Biological invasions by exotic grasses, the grass/fire cycle, and global change: Annual Review of Ecology and Systematics, v. 23, p. 63–87, https://doi.org/10.1146/annurev.es.23.110192.000431.

DeCelles, P., Carrapa, B., Horton, B., and Gehrels, G., 2011, Cenozoic foreland basin system in the central Andes of northwestern Argentina: Implications for Andean geodynamics and modes of deformation: Tectonics, v. 30, no. 6, TC6013, https://doi.org/10.1029/2011TC002948.

Del Papa, C., Disalvo, A., Reynolds, J., Pereyra, R., and Viramonte, J., 1993, Utilización de niveles piroclásticos en correlación estratigráfica: Un ejemplo para el Terciario Superior del noroeste argentino, in 12th Congreso Geológico Argentino y 2nd Congreso de Exploración de Hidrocarburos, Actas, Volume 2: Mendoza, Argentina, Asociación Geológica Argentina, p. 166–171.

Denis, E.H., Pedentchouk, N., Schouten, S., Pagani, M., and Freeman, K.H., 2017, Fire and ecosystem change in the Arctic across the Paleocene–Eocene thermal maximum: Earth and Planetary Science Letters, v. 467, p. 149–156, https://doi.org/10.1016/j.epsl.2017.03.021.

Diefendorf, A.F., Mueller, K.E., Wing, S.L., Koch, P.L., and Freeman, K.H., 2010, Global patterns in leaf 13C discrimination and implications for studies of past and future climate: Proceedings of the National Academy of Sciences of the United States of America, v. 107, no. 13, p. 5738–5743, https://doi.org/10.1073/pnas.0910513107.

Díaz, J.I., and Malizzia, D.C., 1983, Estudio geológico y sedimentológico del Terciario Superior del valle Calchaquí (departamento de San Carlos, provincia de Salta): Boletino de Sedimentológia, v. 2, p. 8–28.

Dupont, L.M., Rommerskirchen, F., Mollenhauer, G., and Schefuß, E., 2013, Miocene to Pliocene changes in South African hydrology and vegetation in relation to the expansion of C4 plants: Earth and Planetary Science Letters, v. 375, p. 408–417, https://doi.org/10.1016/j.epsl.2013.06.005.

Edwards, E.J., and Smith, S.A., 2010, Phylogenetic analyses reveal the shady history of C4 grasses: Proceedings of the National Academy of Sciences of the United States of America, v. 107, no. 6, p. 2532–2537, https://doi.org/10.1073/pnas.0909672107.

Edwards, E.J., and Still, C.J., 2008, Climate, phylogeny and the ecological distribution of C4 grasses: Ecology Letters, v. 11, no. 3, p. 266–276, https://doi.org/10.1111/j.1461-0248.2007.01144.x.

Edwards, E.J., et al., 2010, The origins of C4 grasslands: Integrating evolutionary and ecosystem science: Science, v. 328, p. 587–591, https://doi.org/10.1126/science.1177216.

Ehleringer, J.R., and Cerling, T.E., 2002, C3 and C4 photosynthesis, *in* Mooney, H.A., and Canadell, J.G., eds., Encyclopedia of Global Environmental Change, Volume 2: The Earth System: Biological and Ecological Dimensions of Global Environmental Change: New York, Wiley, p. 186–190.

Ehleringer, J.R., and Monson, R.K., 1993, Evolutionary and ecological aspects of photosynthetic pathway variation: Annual Review of Ecology and Systematics, v. 24, no. 1, p. 411–439, https://doi.org/10.1146/annurev.es.24.110193.002211.

Ehleringer, J.R., Sage, R.F., Flanagan, L.B., and Pearcy, R.W., 1991, Climate change and the evolution of C4 photosynthesis: Trends in Ecology & Evolution, v. 6, no. 3, p. 95–99, https://doi.org/10.1016/0169-5347(91)90183-X.

Ercoli, M.D., Ramírez, M.A., Morales, M.M., Álvarez, A., and Candela, A.M., 2019, First record of Carnivora (Puma lineage, Felidae) in the Uquía Formation (late Pliocene–early Pleistocene, NW Argentina) and its significance in the Great American biotic interchange: Ameghiniana, v. 56, no. 3, p. 195–212, https://doi.org/10.5710/AMGH.31.03.2019.3206.

Feakins, S.J., 2013, Pollen-corrected leaf wax D/H reconstructions of northeast African hydrological changes during the late Miocene: Palaeogeography, Palaeoclimatology, Palaeoecology, v. 374, p. 62–71, https://doi.org/10.1016/j.palaeo.2013.01.004.

Feakins, S.J., Liddy, H.M., Tauxe, L., Galy, V., Feng, X., Tierney, J.E., Miao, Y., and Warny, S., 2020, Miocene C4 grassland expansion as recorded by the Indus Fan: Paleoceanography and Paleoclimatology, v. 35, no. 6, https://doi.org/10.1029/2020PA003856.

Fick, S.E., and Hijmans, R.J., 2017, WorldClim 2: New 1-km spatial resolution climate surfaces for global land areas: International Journal of Climatology, v. 37, no. 12, p. 4302–4315, https://doi.org/10.1002/joc.5086.

Fox, D.L., and Koch, P.L., 2003, Tertiary history of C4 biomass in the Great Plains, USA: Geology, v. 31, no. 9, p. 809–812, https://doi.org/10.1130/G19580.1.

Fredlund, G.G., and Tieszen, L.T., 1994, Modern phytolith assemblages from the North American Great Plains: Journal of Biogeography, v. 21, p. 321–335, https://doi.org/10.2307/2845533.

Freeman, K., and Colarusso, L., 2001, Molecular and isotopic records of C4 grassland expansion in the late Miocene: Geochimica et Cosmochimica Acta, v. 65, no. 9, p. 1439–1454, https://doi.org/10.1016/S0016-7037(00)00573-1.

Gallagher, T.M., and Sheldon, N.D., 2013, A new paleothermometer for forest paleosols and its implications for Cenozoic climate: Geology, v. 41, no. 6, p. 647–650, https://doi.org/10.1130/G34074.1.

Galli, C.I., Alonso, R.N., and Coira, L.B., 2017, Integrated stratigraphy of the Cenozoic Andean foreland basin (northern Argentina), in Ambrosino, G.A., ed., Seismic and Sequence Stratigraphy and Integrated Stratigraphy—New Insights and Contributions: London, UK, InTechOpen, p. 129–156, https://doi.org/10.5772/intechopen.69985.

Galli, C.I., Alonso, R.N., and Coira, B.L., 2023, Paleoenvironmental evolution of the Cenozoic foreland basin to intermontane basins in the Eastern Cordillera, northwestern Argentina: Journal of South American Earth Sciences, v. 130, https://doi.org/10.1016/j.jsames.2023.104582.

Ghosh, A., 2021, Did Changes in Seasonality and Fire Frequency Cause C4 Grass Expansion in South America?: Investigations from N.W. Argentina Using Geochemical Proxies for Climate and Vegetation Change [M.S. thesis]: Northridge, California, California State University–Northridge, 167 p., http://dspace.calstate.edu/handle/10211.3/219787 (accessed September 2024).

Gowik, U., and Westhoff, P., 2011, The path from C3 to C4 photosynthesis: Plant Physiology, v. 155, no. 1, p. 56–63, https://doi.org/10.1104/pp.110.165308.

Griffin, D.L., 2002, Aridity and humidity: Two aspects of the late Miocene climate of North Africa and the Mediterra-

nean: Palaeogeography, Palaeoclimatology, Palaeoecology, v. 182, no. 1–2, p. 65–91, https://doi.org/10.1016/S0031-0182(01)00453-9.

Hain, M.P., Strecker, M.R., Bookhagen, B., Alonso, R.N., Pingel, H., and Schmitt, A.K., 2011, Neogene to Quaternary broken foreland formation and sedimentation dynamics in the Andes of NW Argentina (25°S): Tectonics, v. 30, no. 2, TC2006, https://doi.org/10.1029/2010TC002703.

Hatano, N., and Yoshida, K., 2017, Sedimentary environment and paleosols of middle Miocene fluvial and lacustrine sediments in central Japan: Implications for paleoclimate interpretations: Sedimentary Geology, v. 347, p. 117–129, https://doi.org/10.1016/j.sedgeo.2016.11.004.

Hatch, M.D., 1987, C4 photosynthesis: A unique blend of modified biochemistry, anatomy and ultrastructure: Biochimica et Biophysica Acta (BBA)—Reviews on Bioenergetics, v. 895, no. 2, p. 81–106, https://doi.org/10.1016/S0304-4173(87)80009-5.

Heppenheimer, H., Steffens, K., Püttman, W., and Kalkreuth, W., 1992, Comparison of resinite-related aromatic biomarker distributions in Cretaceous–Tertiary coals from Canada and Germany: Organic Geochemistry, v. 18, no. 3, p. 273–287, https://doi.org/10.1016/0146-6380(92)90069-A.

Herbert, T.D., Lawrence, K.T., Tzanova, A., Peterson, L.C., Caballero-Gill, R., and Kelly, C.S., 2016, Late Miocene global cooling and the rise of modern ecosystems: Nature Geoscience, v. 9, no. 11, p. 843–847, https://doi.org/10.1038/ngeo2813.

Higgins, S.I., and Scheiter, S., 2012, Atmospheric CO2 forces abrupt vegetation shifts locally, but not globally: Nature, v. 488, p. 209–212, https://doi.org/10.1038/nature11238.

Hoetzel, S., Dupont, L., Schefuß, E., Rommerskirchen, F., and Wefer, G., 2013, The role of fire in Miocene to Pliocene C4 grassland and ecosystem evolution: Nature Geoscience, v. 6, no. 12, p. 1027–1030, https://doi.org/10.1038/ngeo1984.

Horton, B.K., 2018, Sedimentary record of Andean mountain building: Earth-Science Reviews, v. 178, p. 279–309, https://doi.org/10.1016/j.earscirev.2017.11.025.

Huang, Y., Clemens, S.C., Liu, W., Wang, Y., and Prell, W.L., 2007, Large-scale hydrological change drove the late Miocene C4 plant expansion in the Himalayan foreland and Arabian Peninsula: Geology, v. 35, no. 6, p. 531–534, https://doi.org/10.1130/G23666A.1.

Hui, Z., Gowan, E.J., Hou, Z., Zhou, X., Ma, Y., Guo, Z., and Zhang, J., 2021, Intensified fire activity induced by aridification facilitated late Miocene C4 plant expansion in the northeastern Tibetan Plateau, China: Palaeogeography, Palaeoclimatology, Palaeoecology, v. 573, https://doi.org/10.1016/j.palaeo.2021.110437.

Hyland, E.G., and Sheldon, N.D., 2013, Coupled CO2-climate response during the early Eocene climatic optimum: Palaeogeography, Palaeoclimatology, Palaeoecology, v. 369, p. 125–135, https://doi.org/10.1016/j.palaeo.2012.10.011.

Hyland, E.G., and Sheldon, N.D., 2016, Examining the spatial consistency of palaeosol proxies: Implications for palaeoclimatic and palaeoenvironmental reconstructions in terrestrial sedimentary basins: Sedimentology, v. 63, no. 4, p. 959–971, https://doi.org/10.1111/sed.12245.

Hyland, E.G., Sheldon, N.D., Smith, S.Y., and Strömberg, C.A., 2019, Late Miocene rise and fall of C4 grasses in the western United States linked to aridification and uplift: Geological Society of America Bulletin, v. 131, no. 1–2, p. 224–234, https://doi.org/10.1130/B32009.1.

Hyland, E., Berry, K., Azmi, I., Cardenal, E., and Burgener, L., 2023, Statistical package for estimating uncertainty on phytolith counts using bootstrapping analyses (version 2023): Zenodo, https://doi.org/10.5281/zenodo.8347036.

Hynek, S.A., Passey, B.H., Prado, J.L., Brown, F.H., Cerling, T.E., and Quade, J., 2012, Small mammal carbon isotope ecology across the Miocene-Pliocene boundary, northwestern Argentina: Earth and Planetary Science Letters, v. 321–322, p. 177–188, https://doi.org/10.1016/j.epsl.2011.12.038.

Insel, N., Poulsen, C.J., and Ehlers, T.A., 2010, Influence of the Andes Mountains on South American moisture transport, convection, and precipitation: Climate Dynamics, v. 35, p. 1477–1492, https://doi.org/10.1007/s00382-009-0637-1.

Insel, N., Poulsen, C.J., Ehlers, T.A., and Sturm, C., 2012, Response of meteoric δ18O to surface uplift—Implications for Cenozoic Andean Plateau growth: Earth and Planetary Science Letters, v. 317–318, p. 262–272, https://doi.org/10.1016/j.epsl.2011.11.039.

Intergovernmental Panel on Climate Change (IPCC), 2014, Climate Change 2014 Synthesis Report: Geneva, Switzerland, Intergovernmental Panel on Climate Change, p. 1059–1072.

Kappenberg, A., Braun, M., Amelung, W., and Lehndorff, E., 2019, Fire condensates and charcoals: Chemical composition and fuel source identification: Organic Geochemistry, v. 130, p. 43–50, https://doi.org/10.1016/j.orggeochem.2019.01.009.

Karp, A.T., Behrensmeyer, A.K., and Freeman, K.H., 2018, Grassland fire ecology has roots in the late Miocene: Proceedings of the National Academy of Sciences of the United States of America, v. 115, no. 48, p. 12,130–12,135, https://doi.org/10.1073/pnas.1809758115.

Karp, A.T., Holman, A.I., Hopper, P., Grice, K., and Freeman, K.H., 2020, Fire distinguishers: Refined interpretations of polycyclic aromatic hydrocarbons for paleo-applications: Geochimica et Cosmochimica Acta, v. 289, p. 93–113, https://doi.org/10.1016/j.gca.2020.08.024.

Karp, A.T., Uno, K.T., Polissar, P.J., and Freeman, K.H., 2021a, Late Miocene C4 grassland fire feedbacks on the Indian subcontinent: Paleoceanography and Paleoclimatology, v. 36, no. 4, https://doi.org/10.1029/2020PA004106.

Karp, A.T., Andrae, J.W., McInerney, F.A., Polissar, P.J., and Freeman, K.H., 2021b, Soil carbon loss and weak fire feedbacks during Pliocene C4 grassland expansion in Australia: Geophysical Research Letters, v. 48, no. 2, https://doi.org/10.1029/2020GL090964.

Keeley, J.E., and Rundel, P.W., 2005, Fire and the Miocene expansion of C4 grasslands: Ecology Letters, v. 8, no. 7, p. 683–690, https://doi.org/10.1111/j.1461-0248.2005.00767.x.

Kleinert, K., and Strecker, M.R., 2001, Climate change in response to orographic barrier uplift: Paleosol and stable isotope evidence from the late Neogene Santa Maria basin, northwestern Argentina: Geological Society of America Bulletin, v. 113, no. 6, p. 728–742, https://doi.org/10.1130/0016-7606(2001)113<0728:CCIRTO>2.0.CO;2.

Knorr, G., Butzin, M., Micheels, A., and Lohmann, G., 2011, A warm Miocene climate at low atmospheric CO2 levels: Geophysical Research Letters, v. 38, no. 20, L20701, https://doi.org/10.1029/2011GL048873.

Krull, E.G., and Bray, S.S., 2005, Assessment of vegetation change and landscape variability by using stable carbon isotopes of soil organic matter: Australian Journal of Botany, v. 53, no. 7, p. 651–661, https://doi.org/10.1071/BT04124.

Krull, E.S., Bestland, E.A., and Gates, W.P., 2002, Soil organic matter decomposition and turnover in a tropical Ultisol: Evidence from δ13C, δ15N and geochemistry: Radiocarbon, v. 44, no. 1, p. 93–112, https://doi.org/10.1017/S0033822200064705.

Kumar, M., Saikia, K., Agrawal, S., Ghosh, R., Ali, S.N., Arif, M., et al., 2022, Climatic control on the C3 and C4 plant abundance during the late Pleistocene–Holocene in the northern Gangetic Plain, India: Palaeogeography, Palaeoclimatology, Palaeoecology, v. 591, https://doi.org/10.1016/j.palaeo.2022.110890.

Latorre, C., Quade, J., and McIntosh, W.C., 1997, The expansion of C4 grasses and global change in the late Miocene: Stable isotope evidence from the Americas: Earth and Planetary Science Letters, v. 146, no. 1–2, p. 83–96, https://doi.org/10.1016/S0012-821X(96)00231-2.

Latrubesse, E.M., Cozzuol, M., da Silva-Caminha, S.A., Rigsby, C.A., Absy, M.L., and Jaramillo, C., 2010, The late Miocene paleogeography of the Amazon Basin and the evolution of the Amazon River system: Earth-Science Reviews, v. 99, no. 3–4, p. 99–124, https://doi.org/10.1016/j.earscirev.2010.02.005.

Lau, E.V., Gan, S., and Ng, H.K., 2010, Extraction techniques for polycyclic aromatic hydrocarbons in soils: International Journal of Analytical Chemistry, v. 2010, https://doi.org/10.1155/2010/398381.

Lee, D.D., and Seung, H.S., 1999, Learning the parts of objects by non-negative matrix factorization: Nature, v. 401, no. 6755, p. 788–791, https://doi.org/10.1038/44565.

Leegood, R.C., 2000, Transport during C4 photosynthesis, *in* Leegood, R.C., Sharkey, T.D., and von Caemmerer, S., eds., Photosynthesis: Dordrecht, Netherlands, Springer, Advances in Photosynthesis and Respiration 9, p. 459–469, https://doi.org/10.1007/0-306-48137-5_1.

Li, J., Wang, G., Liu, X., Han, J., Liu, M., and Liu, X., 2009, Variations in carbon isotope ratios of C3 plants and distribution of C4 plants along an altitudinal transect on the eastern slope of Mount Gongga: Science in China, Series D: Earth Sciences, v. 52, p. 1714–1723, https://doi.org/10.1007/s11430-009-0170-4.

Lu, J., Algeo, T.J., Zhuang, G., Yang, J., Xiao, G., Liu, J., Huang, J., and Xie, S., 2020, The early Pliocene global expansion of C4 grasslands: A new organic carbon-isotopic dataset from the north China plain: Palaeogeography, Palaeoclimatology, Palaeoecology, v. 538, https://doi.org/10.1016/j.palaeo.2019.109454.

Lukens, W.E., Stinchcomb, G.E., Nordt, L.C., Kahle, D.J., Driese, S.G., and Tubbs, J.D., 2019, Recursive partitioning improves paleosol proxies for rainfall: American Journal of Science, v. 319, no. 10, p. 819–845, https://doi.org/10.2475/10.2019.01.

Luo, X., Zhou, H., Satriawan, T.W., Tian, J., Zhao, R., Keenan, T.F., Griffith, D.M., Sitch, S., Smith, N.G., and Still, C.J., 2024, Mapping the global distribution of C4 vegetation using observations and optimality theory: Nature Communications, v. 15, https://doi.org/10.1038/s41467-024-45606-3.

MacFadden, B.J., Cerling, T.E., and Prado, J., 1996, Cenozoic terrestrial ecosystem evolution in Argentina: Evidence from carbon isotopes of fossil mammal teeth: Palaios, v. 11, no. 4, p. 319–327, https://doi.org/10.2307/3515242.

Mack, G.H., James, W.C., and Monger, H.C., 1993, Classification of paleosols: Geological Society of America Bulletin, v. 105, no. 2, p. 129–136, https://doi.org/10.1130/0016-7606(1993)105<0129:COP>2.3.CO;2.

Madella, M., Alexandre, A., and Ball, T., 2005, International Code for Phytolith Nomenclature 1.0: Annals of Botany, v. 96, no. 2, p. 253–260, https://doi.org/10.1093/aob/mci172.

Marbut, C.F., 1935, Atlas of American Agriculture: Part III, Soils of the United States: Washington, D.C., U.S. Government Printing Office, 98 p.

Miall, A.D., 2014, Fluvial Depositional System: Cham, Switzerland, Springer, 316 p., https://doi.org/10.1007/978-3-319-00666-6.

Miao, Y., et al., 2022, Wildfire history and savanna expansion across southern Africa since the late Miocene: Palaeogeography, Palaeoclimatology, Palaeoecology, v. 603, https://doi.org/10.1016/j.palaeo.2022.111189.

Michel, L.A., Tabor, N.J., and Montañez, I.P., 2016, Paleosol diagenesis and its deep-time paleoenvironmental implications, Pennsylvanian–Permian Lodeve Basin, France: Journal of Sedimentary Research, v. 86, no. 7, p. 813–829, https://doi.org/10.2110/jsr.2016.41.

Michel, L.A., Sheldon, N.D., Myers, T.S., and Tabor, N.J., 2022, Assessment of pretreatment methods on CIA-K and CALMAG indices and the effects on paleoprecipitation estimates: Palaeogeography, Palaeoclimatology, Palaeoecology, v. 601, https://doi.org/10.1016/j.palaeo.2022.111102.

Mulch, A., Uba, C.E., Strecker, M.R., Schoenberg, R., and Chamberlain, C.P., 2010, Late Miocene climate variability and surface elevation in the central Andes: Earth and Planetary Science Letters, v. 290, no. 1–2, p. 173–182, https://doi.org/10.1016/j.epsl.2009.12.019.

Neumann, K., Strömberg, C.A.E., Ball, T., Albert, R.M., Vrydaghs, L., and Cummings, L.S., 2019, International Code for Phytolith Nomenclature (ICPN) 2.0: Annals of Botany, v. 124, no. 2, p. 189–199, https://doi.org/10.1093/aob/mcz064.

Osborne, C.P., 2008, Atmosphere, ecology and evolution: What drove the Miocene expansion of C4 grasslands-Journal of Ecology, v. 96, p. 35–45, https://doi.org/10.1111/j.1365-2745.2007.01323.x.

Osborne, C.P., and Beerling, D.J., 2005, Nature's green revolution: the remarkable evolutionary rise of C4

plants: Pliosophical Transactions of the Royal Society B: Biological Sciences, v. 361, no. 1465, p. 173–194, https://doi.org/10.1098/rstb.2005.1737.

Pagani, M., Arthur, M.A., and Freeman, K.H., 1999, Miocene evolution of atmospheric carbon dioxide: Paleoceanography, v. 14, no. 3, p. 273–292, https://doi.org/10.1029/1999PA900006.

Pagani, M., Zachos, J.C., Freeman, K.H., Tipple, B., and Bohaty, S., 2005, Marked decline in atmospheric carbon dioxide concentrations during the Paleogene: Science, v. 309, p. 600–603, https://doi.org/10.1126/science.1110063.

Passey, B.H., Ayliffe, L.K., Kaakinen, A., Zhang, Z., Eronen, J.T., Zhu, Y., Zhou, L., Cerling, T.E., and Fortelius, M., 2009, Strengthened East Asian summer monsoons during a period of high-latitude warmth?: Isotopic evidence from Mio-Pliocene fossil mammals and soil carbonates from northern China: Earth and Planetary Science Letters, v. 277, no. 3–4, p. 443–452, https://doi.org/10.1016/j.epsl.2008.11.008.

Pearson, P.N., and Palmer, M.R., 2000, Atmospheric carbon dioxide concentrations over the past 60 million years: Nature, v. 406, p. 695–699, https://doi.org/10.1038/35021000.

Peppe, D.J., et al., 2023, Oldest evidence of abundant C4 grasses and habitat heterogeneity in eastern Africa: Science, v. 380, p. 173–177, https://doi.org/10.1126/science.abq2834.

Pingel, H., Mulch, A., Alonso, R.N., Cottle, J., Hynek, S.A., Poletti, J., Rohrmann, A., Schmitt, A.K., Stockli, D.F., and Strecker, M.R., 2016, Surface uplift and convective rainfall along the southern Central Andes (Angastaco Basin, NW Argentina): Earth and Planetary Science Letters, v. 440, p. 33–42, https://doi.org/10.1016/j.epsl.2016.02.009.

Powell, R.L., and Still, C.J., 2009, Biogeography of C_3 and C_4 vegetation in South America, *in* Anais XIV Simpósio Brasileiro de Sensoriamento Remoto: Natal, Brazil, Instituto Nacional de Pesquisas Espaciais, p. 2935–2942.

Quade, J., Cater, J.M., Ojha, T.P., Adam, J., and Mark Harrison, T., 1995, Late Miocene environmental change in Nepal and the northern Indian subcontinent: Stable isotopic evidence from paleosols: Geological Society of America Bulletin, v. 107, no. 12, p. 1381–1397,, https://doi.org/10.1130/0016-7606(1995)107<1381:LMECIN>2.3.CO;2.

Raghavendra, A.S., and Sage, R.F., 2010, C4 Photosynthesis and Related CO2 Concentrating Mechanisms: Dordrecht, Netherlands, Springer, Advances in Photosynthesis and Respiration (AIPH) 32, 412 p.

Ramdahl, T., 1983, Retene—A molecular marker of wood combustion in ambient air: Nature, v. 306, p. 580–582, https://doi.org/10.1038/306580a0.

Ramos, V.A., 2009, Anatomy and global context of the Andes: Main geologic features and the Andean orogenic cycle, *in* Kay, S.M., Ramos, V.A., and Dickinson, W.R., eds., Backbone of the Americas: Shallow Subduction, Plateau Uplift, and Ridge and Terrane Collision: Geological Society of America Memoir 204, p. 31–65, https://doi.org/10.1130/2009.1204(02).

Retallack, G.J., 1988, Field recognition of paleosols, *in* Reinhardt, J., and Sigleo, W.R., eds., Paleosols and Weathering Through Geologic Time: Principles and Applications: Geological Society of America Special Paper 216, p. 1–20, https://doi.org/10.1130/SPE216-p1.

Retallack, G.J., 1991, Untangling the effects of burial alteration and ancient soil formation: Annual Review of Earth and Planetary Sciences, v. 19, p. 183–206, https://doi.org/10.1146/annurev.ea.19.050191.001151.

Retallack, G.J., 1994, The environmental factor approach to the interpretation of paleosols, *in* Amundson, A., Harden, J., and Singer, M., eds., Factors of Soil Formation: A Fiftieth Anniversary Retrospective: Soil Science Society of America Special Publication 33, p. 31–64, https://doi.org/10.2136/sssaspecpub33.c3.

Retallack, G.J., 2005, Pedogenic carbonate proxies for amount and seasonality of precipitation in paleosols: Geology, v. 33, no. 4, p. 333–336, https://doi.org/10.1130/G21263.1.

Retallack, G.J., 2007, Cenozoic paleoclimate on land in North America: The Journal of Geology, v. 115, no. 3, p. 271–294, https://doi.org/10.1086/512753.

Retallack, G.J., 2008, Soils of the Past: An Introduction to Paleopedology: New York, John Wiley and Sons, 552 p.

Reynolds, J.H., Galli, C.I., Hernández, R.M., Idleman, B.D., Kotila, J.M., Hilliard, R.V., and Naeser, C.W., 2000, Middle Miocene tectonic development of the transition zone, Salta Province, northwest Argentina: Magnetic stratigraphy from the Metan Subgroup, Sierra de Gonzalez: Geological Society of America Bulletin, v. 112, no. 11, p. 1736–1751, https://doi.org/10.1130/0016-7606(2000)112<1736:MMTDOT>2.0.CO;2.

Rohrmann, A., Sachse, D., Mulch, A., Pingel, H., Tofelde, S., Alonso, R.N., and Strecker, M.R., 2016, Miocene orographic uplift forces rapid hydrological change in the southern central Andes: Scientific Reports, v. 6, https://doi.org/10.1038/srep35678.

Rossiter, N.A., Setterfield, S.A., Douglas, M.M., and Hutley, L.B., 2003, Testing the grass-fire cycle: Alien grass invasion in the tropical savannas of northern Australia: Diversity & Distributions, v. 9, no. 3, p. 169–176, https://doi.org/10.1046/j.1472-4642.2003.00020.x.

Saarinen, J., Mantzouka, D., and Sakala, J., 2020, Aridity, cooling, open vegetation, and the evolution of plants and animals during the Cenozoic, *in* Martinetto, E., Tschopp, E., and Gastaldo, R.A., eds., Nature through Time: Cham, Switzerland, Springer, Springer Textbooks in Earth Sciences, Geography and Environment, p. 83–107, https://doi.org/10.1007/978-3-030-35058-1_3.

Sage, R.F., 2001, Environmental and evolutionary preconditions for the origin and diversification of the C4 photosynthetic syndrome: Plant Biology, v. 3, no. 3, p. 202–213, https://doi.org/10.1055/s-2001-15206.

Sage, R.F., 2004, The evolution of C4 photosynthesis: The New Phytologist, v. 161, no. 2, p. 341–370, https://doi.org/10.1111/j.1469-8137.2004.00974.x.

Sage, R.F., Sage, T.L., and Kocacinar, F., 2012, Photorespiration and the evolution of C4 photosynthesis: Annual Review of Plant Biology, v. 63, p. 19–47, https://doi.org/10.1146/annurev-arplant-042811-105511.

Scheiter, S., Higgins, S.I., Osborne, C.P., Bradshaw, C., Lunt, D., Ripley, B.S., Taylor, L.L., and Beerling, D.J., 2012, Fire and fire-adapted vegetation promoted C4 expansion in the late Miocene: The New Phytologist, v. 195, no. 3, p. 653–666, https://doi.org/10.1111/j.1469-8137.2012.04202.x.

Scherer, C.M., Lavina, E.L., Dias Filho, D.C., Oliveira, F.M., Bongiolo, D.E., and Aguiar, E.S., 2007, Stratigraphy and facies architecture of the fluvial-aeolian-lacustrine Sergi Formation (Upper Jurassic), Recôncavo Basin, Brazil: Sedimentary Geology, v. 194, no. 3–4, p. 169–193, https://doi.org/10.1016/j.sedgeo.2006.06.002.

Scherer, C.M., Goldberg, K., and Bardola, T., 2015, Facies architecture and sequence stratigraphy of an early post-rift fluvial succession, Aptian Barbalha Formation, Araripe Basin, northeastern Brazil: Sedimentary Geology, v. 322, p. 43–62, https://doi.org/10.1016/j.sedgeo.2015.03.010.

Sepulchre, P., Ramstein, G., Fluteau, F., Schuster, M., Tiercelin, J.J., and Brunet, M., 2006, Tectonic uplift and eastern Africa aridification: Science, v. 313, p. 1419–1423, https://doi.org/10.1126/science.1129158.

Sheldon, N.D., 2006, Abrupt chemical weathering increase across the Permian-Triassic boundary: Palaeogeography, Palaeoclimatology, Palaeoecology, v. 231, no. 3–4, p. 315–321, https://doi.org/10.1016/j.palaeo.2005.09.001.

Sheldon, N.D., and Tabor, N.J., 2009, Quantitative paleoenvironmental and paleoclimatic reconstruction using paleosols: Earth-Science Reviews, v. 95, no. 1–2, p. 1–52, https://doi.org/10.1016/j.earscirev.2009.03.004.

Sheldon, N.D., Retallack, G.J., and Tanaka, S., 2002, Geochemical climofunctions from North American soils and application to paleosols across the Eocene-Oligocene boundary in Oregon: The Journal of Geology, v. 110, no. 6, p. 687–696, https://doi.org/10.1086/342865.

Sheldon, N.D., Smith, S.Y., Stein, R., and Ng, M., 2020, Carbon isotope ecology of gymnosperms and implications for paleoclimatic and paleoecological studies: Global and Planetary Change, v. 184, https://doi.org/10.1016/j.gloplacha.2019.103060.

Simoneit, B.R., and Mazurek, M.A., 1982, Organic matter of the troposphere—II. Natural background of biogenic lipid matter in aerosols over the rural western United States: Atmospheric Environment, v. 16, no. 9, p. 2139–2159, https://doi.org/10.1016/0004-6981(82)90284-0.

Simoneit, B.R., Rogge, W.F., Mazurek, M.A., Standley, L.J., Hildemann, L.M., and Cass, G.R., 1993, Lignin pyrolysis products, lignans, and resin acids as specific tracers of plant classes in emissions from biomass combustion: Environmental Science & Technology, v. 27, no. 12, p. 2533–2541, https://doi.org/10.1021/es00048a034.

Smiley, T.M., Hyland, E.G., Cotton, J.M., and Reynolds, R.E., 2018, Evidence of early C4 grasses, habitat heterogeneity, and faunal response during the Miocene climatic optimum in the Mojave region: Palaeogeography, Palaeoclimatology, Palaeoecology, v. 490, p. 415–430, https://doi.org/10.1016/j.palaeo.2017.11.020.

Sobolev, S.V., Babeyko, A.Y., Koulakov, I., and Oncken, O., 2006, Mechanism of the Andean orogeny: Insight from numerical modeling, *in* Oncken, O., et al., eds., The Andes: Active Subduction Orogeny: Berlin, Springer, Frontiers in Earth Sciences, p. 513–535, https://doi.org/10.1007/978-3-540-48684-8_25.

Soil Survey Staff, 2014, Keys to Soil Taxonomy (12th ed.): Washington, D.C., U.S. Department of Agriculture Natural Resources Conservation Service, 360 p.

Spicer, R.A., 2017, Tibet, the Himalaya, Asian monsoons and biodiversity—In what ways are they related?: Plant Diversity, v. 39, no. 5, p. 233–244, https://doi.org/10.1016/j.pld.2017.09.001.

Starck, D., and Anzótegui, L.M., 2001, The late Miocene climatic change—Persistence of a climatic signal through the orogenic stratigraphic record in northwestern Argentina: Journal of South American Earth Sciences, v. 14, no. 7, p. 763–774, https://doi.org/10.1016/S0895-9811(01)00066-9.

Starck, D., and Vergani, G., 1996, Desarrollo tecto-sedimentario del Cenozoico en el sur de la Provincia de Salta-Argentina, *in* XIII Congreso Geológico Argentino y III Congreso de Exploración de Hidrocarburos, Actas I: Buenos Aires, Argentina, Asociación Geológica Argentina, p. 433–452.

Steinthorsdottir, M., Coxall, H., De Boer, A., Huber, M., Barbolini, N., Bradshaw, C., Burls, N., Feakins, S., Gasson, E., and Henderiks, J., 2021, The Miocene: The future of the past: Paleoceanography and Paleoclimatology, v. 36, no. 4, https://doi.org/10.1029/2020PA004037.

Stiles, C.A., and Stensvold, K.A., 2008, Loess contribution to soils forming on dolostone in the Driftless Area of Wisconsin: Soil Science Society of America Journal, v. 72, no. 3, p. 650–659, https://doi.org/10.2136/sssaj2007.0112.

Still, C.J., Berry, J.A., Collatz, G.J., and DeFries, R.S., 2003, Global distribution of C3 and C4 vegetation: Carbon cycle implications: Global Biogeochemical Cycles, v. 17, https://doi.org/10.1029/2001GB001807.

Stinchcomb, G.E., Nordt, L.C., Driese, S.G., Lukens, W.E., Williamson, F.C., and Tubbs, J.D., 2016, A data-driven spline model designed to predict paleoclimate using paleosol geochemistry: American Journal of Science, v. 316, no. 8, p. 746–777, https://doi.org/10.2475/08.2016.02.

Strömberg, C.A., 2003, The Origin and Spread of Grass-Dominated Ecosystems during the Tertiary of North American and How It Relates to the Evolution of Hypsodonty in Equids [Ph.D. dissertation]: Berkeley, California, University of California–Berkeley, 1558 p.

Strömberg, C.A., 2004, Using phytolith assemblages to reconstruct the origin and spread of grass-dominated habitats in the Great Plains of North America during the late Eocene to early Miocene: Palaeogeography, Palaeoclimatology, Palaeoecology, v. 207, no. 3–4, p. 239–275, https://doi.org/10.1016/j.palaeo.2003.09.028.

Strömberg, C.A., 2011, Evolution of grasses and grassland ecosystems: Annual Review of Earth and Planetary Sciences, v. 39, p. 517–544, https://doi.org/10.1146/annurev-earth-040809-152402.

Strömberg, C.A., and McInerney, F.A., 2011, The Neogene transition from C3 to C4 grasslands in North America: Assemblage analysis of fossil phytoliths: Paleobiology, v. 37, p. 50–71, https://doi.org/10.1666/09067.1.

Tauxe, L., and Feakins, S.J., 2020, A reassessment of the chronostratigraphy of late Miocene C3-C4 transitions:

Paleoceanography and Paleoclimatology, v. 35, no. 7, https://doi.org/10.1029/2020PA003857.

Tieszen, L.L., Senyimba, M.M., Imbamba, S.K., and Troughton, J.H., 1979, The distribution of C3 and C4 grasses and carbon isotope discrimination along an altitudinal and moisture gradient in Kenya: Oecologia, v. 37, p. 337–350, https://doi.org/10.1007/BF00347910.

Tineo, D.E., Moyano-Paz, D., Varela, A.N., and Poiré, D.G., 2022a, Onset of the Miocene Chaco foreland basin: Depositional conditions, provenance and paleogeographic implications of the Tranquitas Formation (Argentina): International Journal of Earth Sciences, v. 111, no. 6, p. 1739–1771, https://doi.org/10.1007/s00531-022-02203-3.

Tineo, D.E., Comerio, M.A., Vigiani, L.H., Kürten Moreno, G.S., and Poiré, D.G., 2022b, Tectonic and paleoclimatic controls on the composition of inland wetland deposits, Chaco foreland basin, central Andes: Journal of Sedimentary Research, v. 92, no. 2, p. 112–133, https://doi.org/10.2110/jsr.2021.033.

Tipple, B.J., and Pagani, M., 2007, The early origins of terrestrial C4 photosynthesis: Annual Review of Earth and Planetary Sciences, v. 35, p. 435–461, https://doi.org/10.1146/annurev.earth.35.031306.140150.

Tipple, B.J., Meyers, S.R., and Pagani, M., 2010, Carbon isotope ratio of Cenozoic CO2: A comparative evaluation of available geochemical proxies: Paleoceanography, v. 25, PA3202, https://doi.org/10.1029/2009PA001851.

Ulberich, J.P.V., Ercoli, M.D., Álvarez, A., and Constantini, O.E., 2021, New insights on landscape and environmental evolution in the Subandean region, southern Central Andes: Sedimentology and geochronology of Guanaco Formation in the Río Chico (Jujuy, northwestern Argentina): Global and Planetary Change, v. 207, https://doi.org/10.1016/j.gloplacha.2021.103673.

Westerhold, T., et al., 2020, An astronomically dated record of Earth's climate and its predictability over the last 66 million years: Science, v. 369, no. 6509, p. 1383–1387, https://doi.org/10.1126/science.aba6853.

Wynn, J.G., 2007, Carbon isotope fractionation during decomposition of organic matter in soils and paleosols: Implications for paleoecological interpretations of paleosols: Palaeogeography, Palaeoclimatology, Palaeoecology, v. 251, no. 3–4, p. 437–448, https://doi.org/10.1016/j.palaeo.2007.04.009.

Zhou, H., Helliker, B.R., Huber, M., Dicks, A., and Akçay, E., 2018, C4 photosynthesis and climate through the lens of optimality: Proceedings of the National Academy of Sciences of the United States of America, v. 115, no. 47, p. 12,057–12,062, https://doi.org/10.1073/pnas.1718988115.

Zhou, Y., Fan, J., Zhong, H., and Zhang, W., 2013, Relationships between altitudinal gradient and plant carbon isotope composition of grassland communities on the Qinghai-Tibet Plateau, China: Science China Earth Sciences, v. 56, p. 311–320, https://doi.org/10.1007/s11430-012-4498-9.

Zimicz, N., Payrola, P., and del Papa, C., 2018, New, late Miocene mammalian assemblage from the Palo Pintado Formation (northwestern Argentina): Journal of South American Earth Sciences, v. 81, p. 31–44, https://doi.org/10.1016/j.jsames.2017.11.003.

Science Editor: Mihai Ducea
Associate Editor: Gregory Henkes

Manuscript Received 23 June 2024
Revised Manuscript Received 30 December 2024
Manuscript Accepted 5 February 2025